MILLIMETER WAVE COMMUNICATIONS

THESIS

AFIT/GE/EE/84J-08 Steven E. Payne
1st Lt USAF

DEPARTMENT OF THE AIR FORCE
AIR UNIVERSITY
AIR FORCE INSTITUTE OF TECHNOLOGY

Wright-Patterson Air Force Base, Ohio

AFIT/GE/EE/84J-08

MILLIMETER WAVE COMMUNICATIONS

THESIS

AFIT/GE/EE/84J-08 Steven E. Payne
1st Lt USAF

MILLIMETER WAVE COMMUNICATIONS

THESIS

Presented to the Faculty of the School of Engineering

of the Air Force Institute of Technology

Air University

in Partial Fulfillment of the

Requirements for the Degree of

Master of Science

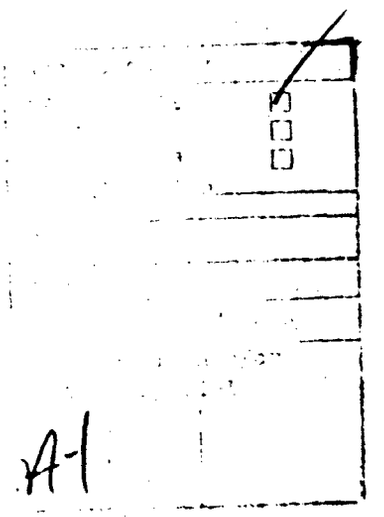

by

Steven E. Payne, B.S.

1st Lt USAF

Graduate Electrical Engineering

June 1984

Acknowledgements

I would like to thank my thesis advisor, Major Ken Castor for proposing this thesis topic. I am extremely grateful for all the patience and guidance I have received from Major Castor during the course of this project.

I want to extend my gratitude to Lieutenant Colonel Ronald Carpinella, Ronald Rudmann, Captain Jim Williams, and Doctor Vic Syed who read the manuscript and made valuable contributions.

Thanks is also due for the outstanding efforts of the typist, Mrs. Sheryl Michel.

Finally, and most importantly, I especially want to express my love to my wife, Georgia, and my daughter, Lauren. Their love, patience, and encouragement made this thesis a special success.

Steven E. Payne

Contents

List of Figures

List of Figures (Continued)

List of Tables

Abstract

This investigation establishes the maximum communication link, i.e., transmitter/receiver separation, available to a millimeter wave channel in a clear, non-turbulent atmosphere for a low-power, low data-rate system. The frequencies considered are from the oxygen resonant absorbtion band centered around 60 GHz for several altitudes to 20 kilometers. The effort is concerned with various modulation schemes for the transmission of digital data and their relative performance in the presence of a jammer.

The analysis is accomplished by taking the Friis communication link equation and accounting for tropospheric absorbtion loss. A Pascal-coded algorithm is developed to assess the relative data transmission performance of the various modulation techniques. The program was written general enough for the user to specify: the carrier frequency, attenuation factor, transmitter power, transmitting and receiving antenna gains, system bandwidth, particular modulation technique, set of range values of interest, jammer power, jammer's antenna gains, and jammer's location.

The results of this investigation indicate that communication links operating at frequencies centered around 60 GHz of the millimeter wave region end rather abruptly due to the inherently high attenuation. Jamming has a limited effect on millimeter wave communications depending upon the frequency. For the frequencies considered, a jammer requires enormous amounts of power and must be positioned "uncomfortably" close to the target receiver to be effective. The application of coherent modulation methods, coding, or spread spectrum techniques as a means to improve the performance of millimeter waves is not required.

Chapter 1: Introduction

Motivation

The 30 to 300 GHz band of the electromagnetic spectrum is commonly called the millimeter wave region. This portion of the spectrum lies above the microwave region and below the electro-optic region. In recent years, advances in the development of transmitters, receivers, devices, and components have drawn increased attention to the millimeter wave region. The expanded development of millimeter wave componentry would provide systems with wide bandwidths to support high data rate users and reduced sensitivity to propagation limitations compared with electro-optical systems. Also, millimeter wave systems would relieve the spectral congestion of the lower frequencies. This region has always held the interest of the research and engineering community since early investigations during the early fifties revealed many potential uses due to the unique characteristics of millimeter waves. These characteristics will be described more fully in Chapter 2. Applications were found in many fields such as radar, communications, and navigation.

Over the last 30 years, there has been much discussion and speculation about these potential applications; yet, the major obstacle to these applications was the available componentry. Efficient sources did not exist. Nor could the vacuum tubes of the day provide reliable power (Reference 1). As an example, using millimeter waves was often considered for point-to-point communication, but these systems were always too expensive. As a result, alternate technology was used. As lasers became operational, emphasis was shifted to developing the optical range leaving the millimeter region practically disregarded

(Reference 2: 15-16).

Today's improved technology is capable of providing a variety of devices in the millimeter wave region. For example, solid-state IMPATTs have seen extensive development. These "state-of-the-art" devices now operate to nearly 300 GHz (Reference 3: 125-126). As a result of the component and processing advances, use of these higher frequencies has become an attractive possibility.

Today, there is a genuine need for millimeter systems applications in such fields as radar and navigation, either as a replacement for an electro-optic system or to complement it. There is even a greater potential for military use of millimeter communications. Besides being a region that is wide open for development and that provides greater bandwidth, the frequency dependent attenuation can be put to an advantage. By choosing a frequency that is strongly attenuated by the atmosphere, it would be possible to establish limits on the effective communication link with little signal power falling outside the resulting communication zone. Such a system would operate relatively free from detection, be difficult to jam, and be useful in many short-range, tactical situations. Particular examples are easily imagined for short-range ship-to-ship communication, air-to-air communication, and hand-held battlefield communications.

Problem

The problem investigated in this study is to consider the oxygen absorbtion band centered around 60 GHz in clear, non-turbulent atmosphere for the transmission of digital data and establish an upper limit on the communication zones that should end rather abruptly due to

high attenuation. This thesis will compare these results with those operating in the presence of a jammer.

Scope

This effort will be concerned with various modulation schemes in a clear, non-turbulent atmosphere for the transmission of digital data and their relative performance in the presence of a jammer. It will not investigate channel coding techniques, antenna sidelobe reduction, nor cancelling methods such as adaptive echo suppression.

Assumptions

It is initially assumed that the radio path is over a flat earth surface. Typically, in the design of a radio link, either the earth's surface or radio path is assumed to be curved. However, due to the relatively short operating range of millimeter radiation, the straight-line assumption is reasonable and simplifies the geometry. In addition, the radio link is assumed to be free from the effects of fading multipath transmission and intersymbol interference.

Approach

This project can be broken into four major tasks:

1. Initially, the background theory on millimeter wave radiation will be investigated so that an extensive summary of the capabilities and limitations may be presented.
2. Next, this information will be used to model the millimeter wave channel in a clear, non-turbulent atmosphere to set a limit on the

transmission of frequencies centered around 60 GHz.

3. Then, the resulting millimeter wave channel model will be used to examine digital signal transmission at millimeter wave carrier frequencies through the atmosphere.

4. The final task will include an investigation of the above system's susceptibility to jamming. This thesis considers a worst-case scenario consisting of a jammer looking directly into the receiving antenna's main lobe. According to information theory, the most destructive type of additive noise in a communication channel is white Gaussian noise. Thus, the jammer will place bandlimited white Gaussian noise power in each signaling band.

Chapter 2: Millimeter Wave Radiation

Introduction

Frequencies with a wavelength near one millimeter are called, quite simply, millimeter waves. The millimeter wave region includes frequencies from 30 to 300 GHz (10 to 1 mm wavelength). This region is also called the extra-high frequency (EHF) band when using radar terminology. These limits are generally accepted; although, the Institute of Electrical and Electronics Engineers' standard specifies that the 40 to 300 GHz band be designated "Millimeter Waves". They consider those frequencies located between 27 and 40 GHz to be the Ka-Band.

Similar terms are often used for slightly overlapping frequency regions. One of the more common names include "near-millimeter waves" which corresponds to frequencies from 90 to 1000 GHz (3 to 0.3 mm). Another common term, "submillimeter waves", refers to the frequency band from about 150 to 3000 GHz (2 to 0.1 mm). Figure II-1 illustrates these

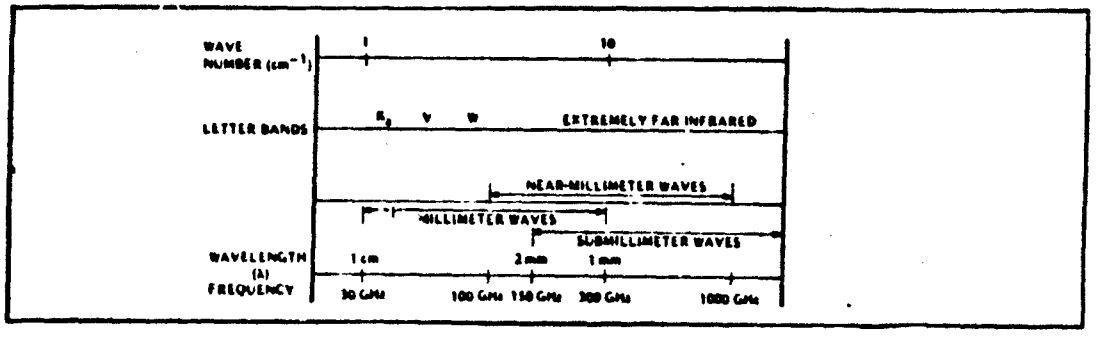

Fig. II-1 Nomenclature for millimeter waves and other frequency ranges (Ref 4: 2).

designations (Reference 4: 2). Another common practice is to include the frequency range between 10 and 30 GHz as part of the millimeter wave region. Although these frequencies do not formally belong to this region, they are frequently considered in connection with millimeter waves because the propagation effects are similar.

This chapter investigates the propagation phenomena which affects the design of communication systems operating at millimeter wave frequencies. First, several important characteristics which are unique to this region are described. Next, certain advantages of interest for electronic communications are listed. Finally, an example is presented which illustrates the high tropospheric absorbtion and short operation range of millimeter waves.

Characteristics of Millimeter Waves

Millimeter waves have three primary characteristics. The application of the millimeter region is dictated by these inherent properties and are listed below:

1. Atmospheric Attenuation. Probably the most important property of millimeter waves are their high attenuation by the atmosphere. Shown in Figure II-2 is the average attenuation produced by clear air at the standard pressure of one atmosphere for 7.5 g/m^3 water vapor at sea level. Also shown in Figure II-2 is the average attenuation at 4 kilometers with 1.0 g/m^3 water vapor. Within the millimeter region, there exists four "propagation windows". These windows occur where the attenuation is at a minimum, located approximately at 35, 95, 140, and 220 GHz.

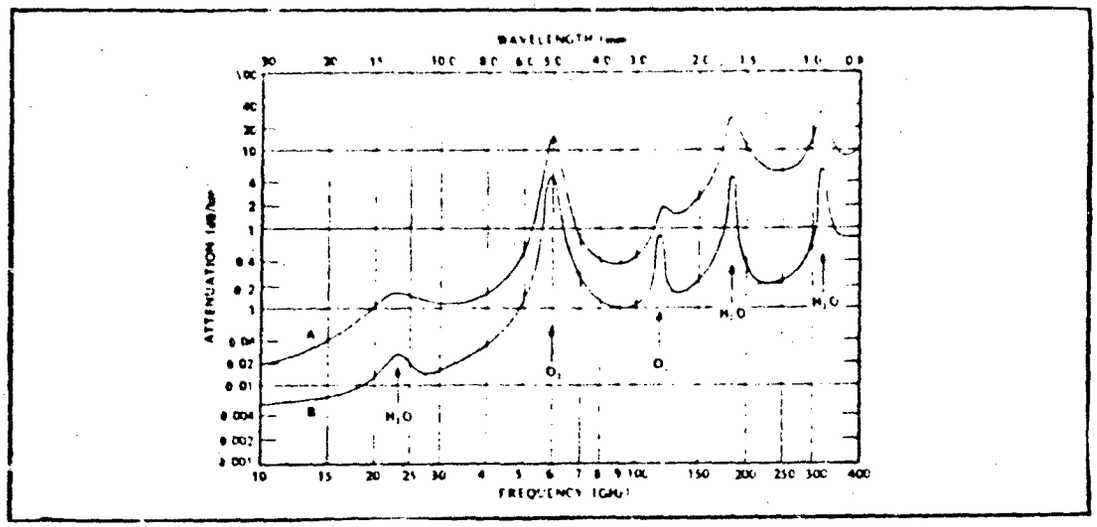

Fig. II-2. Average atmospheric absorbtion of millimeter waves. A: Sea Level; T = 20°C; P = 760 mm; P = 7.5 g/m. B: 4 km; T = 0°C; P = 1 g/m. (Ref 4: 4).

The regions of large attenuation which separate these windows are called "absorbtion bands". These absorbtion bands are produced mostly by molecular resonances of water vapor and oxygen interacting with the millimeter wave. That is, by the laws of quantuum physics, the molecules absorb discrete amounts of energy from the millimeter wave and are excited to a higher energy level. In returning to a lower energy level, they re-emit this energy isotropically. This effectively produces an attenuation of the incident wave (Reference 5: 83-84).

2. Broad Bandwidth. The millimeter region has wide bandwicths available. This is illustrated by considering a ten percent bandwidth at the 60 GHz tropospheric absorbtion band. This band is more than twice the width of the entire UHF band. In fact, the width of the millimeter region is over nine times the width of all the lower frequencies combined (Reference 2: 27). This feature would allow very

high data-rate transmissions and high bandwidth channel coding techniques.

3. Narrow Beamwidth. Since the beamwidth depends on the frequency, size, and type of antenna (Reference 2: 77), for a given antenna size a smaller beamwidth is obtained with millimeter waves than with microwaves. The high degree of directivity associated with narrow beamwidths would help relieve the interference in cross-city communications. A narrow beamwidth reduces errors due to multipath propagation and minimizes losses due to sidelobe returns.

Advantages of Millimeter Waves

The primary characteristics of millimeter waves may provide unique advantages for electronic communications. Three such advantages are listed below:

1. Low Probability-of-Intercept (LPI). Atmospheric attenuation is usually considered to be a disadvantage; however, in short-range covert communication, use of a high absorbtion band will practically reduce propagation overshoot. Thus, concealing the signal from undesired intercept receivers. The degree of concealment is described probabilistically by "probability-of-intercept". High attenuation combined with its narrow beamwidth provide millimeter waves a low probability-of-intercept.

2. High Gain. Antenna gain is inversely proportional to the antenna's beamwidth. Since the millimeter wave antenna possesses a narrow beamwidth, the antenna should also have a high gain. This is easily demonstrated.

The antenna gain and beamwidth equations for a parabolic antenna are

$$G = \frac{(\pi D)^2}{\lambda^2} \eta \qquad (2.1)$$

$$BW = \frac{70\lambda}{D} \qquad (2.2)$$

where

G = antenna gain
η = antenna radiation efficiency
BW = half-power antenna beamwidth
λ = wavelength in meters
D = antenna diameter in meters

Re-arranging equation 2.2 and substituting into equation 2.1 results in

$$G = \frac{70\,\pi^2\,D}{\lambda} \times \frac{1}{BW}. \qquad (2.3)$$

Equation 2.3 illustrates the inverse relation between gain and beamwidth. Table II-1 is a comparison of equations 2.1 and 2.2 for various antenna diameters to demonstrate this relation (Reference 2: 77-78). A typical antenna radiation efficiency of 0.55 is used for convenience.

3. Small Size. Generally, small wavelengths allow small components. This is true for millimeter waves. This becomes especially important when size is a major consideration. For example, satellite, aircraft, and missile systems all demand small size components. Also, hand-held radios capable of providing LPI communication for covert operation are possible by choosing a carrier frequency in the millimeter region.

Table II-1. Antenna gain and beamwidth comparisons (Ref 2: 77).

Antenna Diameter inch (meter)	Operating Frequency 35 GHz	60 GHz	94 GHz
2.0 (0.0508)	22.8 dB Gain	27.5 dB Gain	31.4 dB Gain
	11.8 Degrees	6.9 Degrees	4.4 Degrees
3.0 (0.0762)	26.3 dB Gain	31.0 dB Gain	34.9 dB Gain
	7.9 Degrees	4.6 Degrees	2.9 Degrees
4.0 (0.1016)	28.8 dB Gain	33.5 dB Gain	37.4 dB Gain
	5.9 Degrees	3.4 Degrees	2.2 Degrees
6.0 (0.1524)	32.3 dB Gain	37.0 dB Gain	40.0 dB Gain
	3.9 Degrees	2.3 Degrees	1.5 Degrees
12.0 (0.3048)	38.4 dB Gain	43.0 dB Gain	46.0 dB Gain
	2.0 Degrees	1.1 Degrees	0.7 Degrees

Antenna radiation efficiency (η) is assumed to be 0.55

Atmospheric and Propagation Effects

A number of atmospheric propagation phenomena contribute to the attenuation, phase-shift, and angle-of-arrival variations experienced by radio signals around the millimeter frequency range. The degree of variation in the wave parameters is related to the particular frequency, meteorological conditions, and the geometry of the propagation path. Under certain conditions, the atmospheric effects are insignificant and at other times the effects are severe.

1. Attenuation. The importance of attenuation in the millimeter region cannot be over emphasized. Signal attenuation is caused by some combination of absorbtion and scattering effects.

A. Clear Weather. In clear weather, the primary attenuation factor is the molecular absorbtion of energy by water vapor (H_2O) and oxygen (O_2); scattering effects are negligible. There does exist additional very weak absorbtion from the rotational lines of CO, N_2O, and O_3, but these are insignificant when compared to water vapor (Reference 16: 35). With few exceptions, additional attenuation in clear air due to pollutants, dust, and aerosols are negligible. The average attenuation by a clear atmosphere is shown in Figure II-3. It should be pointed out that there exists some uncertainty associated with the existing data. The problem is that attenuation measurements must be made with reference to a clear weather signal. This clear signal changes with time along with the local meteorological dynamic variations (Reference 4: 37-38). Figure II-3 illustrates this uncertainty by shading the window region two-way attenuation levels. It is interesting to note the large variation at 220 GHz. Here, the clear air attenuation varies from about 1.5 dBm/km to 11 dB/km. Seasonal variations can

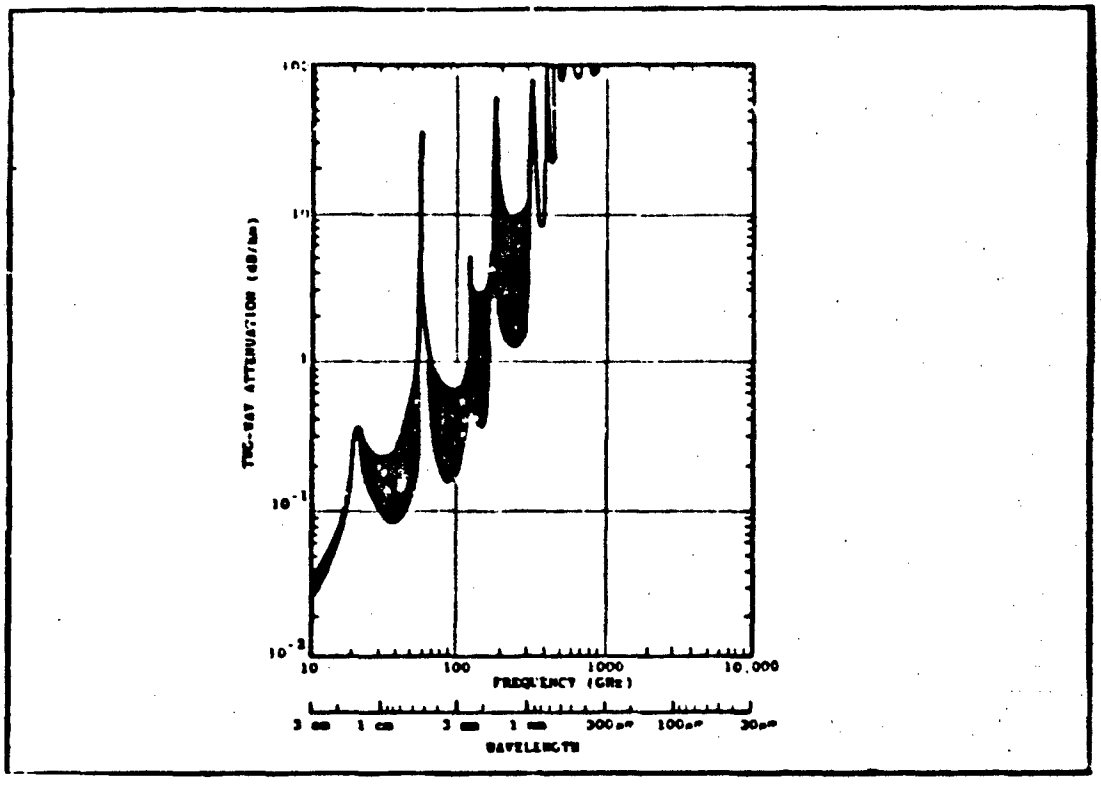

Fig. II-3. Clear weather attenuation uncertainty for horizontal, sea level path (Ref 4: 37)

affect these values by as much as 10 to 15 dB/km (Reference 4: 38). Reduced attenuation is found at higher altitudes. Reber, Mitchell, and Carter (Reference 13: 77-78) have calculated the horizontal attenuation rate around the 60 GHz oxygen resonant absorbtion band for several altitudes to 20 kilometers. Table II-2 lists the attenuation rates at the oxygen resonant frequencies. Table II-3 lists the attenuation rates at frequencies between the resonant lines. The computations in Table II-2 and Table II-3 are accurate to about one percent. For example, a computed attenuation of 100 dB would be accurate to 1 dB.

B. Rain. In recent years, there has been much activity in rain attenuation research. Rain has the ability to cause complete outages

Table II-2. Horizontal attenuation rates in dB/km at oxygen resonant frequencies (Ref 13: 78).

FREQ. (GHz)	Altitude, km 0	4	8	12	16	20
48.4530	0.1683	0.0808	0.0360	0.0171	0.0053	0.0005
48.9582	0.1926	0.0922	0.0409	0.0194	0.0064	0.0006
49.4648	0.2226	0.1061	0.0496	0.0221	0.0075	0.0010
49.9730	0.2607	0.1237	0.0544	0.0256	0.0087	0.0016
50.4830	0.3104	0.1464	0.0639	0.0299	0.0102	0.0020
50.9949	0.3776	0.1772	0.0767	0.0355	0.0123	0.0028
51.5091	0.4722	0.2211	0.0948	0.0434	0.0152	0.0041
52.0259	0.6096	0.2870	0.1226	0.0555	0.0202	0.0069
52.5458	0.8142	0.3905	0.1684	0.0757	0.0296	0.0120
53.0695	1.1218	0.5574	0.2483	0.1128	0.0488	0.0243
53.5960	1.5792	0.8260	0.3895	0.1831	0.0890	0.0518
54.1294	2.2495	1.2526	0.6375	0.3171	0.1714	0.1113
54.6728	3.2103	1.9157	1.0625	0.5661	0.3319	0.2304
55.2214	4.5333	2.9030	1.7560	1.0050	0.6228	0.4501
55.7839	6.3662	4.4549	2.9670	1.8215	1.1457	0.8334
56.2648	8.1019	6.2760	4.9609	3.5406	2.3618	1.5993
56.3634	8.3745	6.4975	5.1476	3.6663	2.4936	1.7639
56.9682	9.6456	7.2875	5.5081	3.8172	2.6531	2.0647
57.6125	11.2650	8.7892	7.0064	5.1039	3.6298	2.8648
58.3239	13.7232	11.9636	10.9883	8.6844	6.0804	4.3993
58.4466	13.9019	12.0384	10.8780	8.4811	5.6843	3.8536
59.1642	14.4034	11.9067	10.0484	7.6391	5.3097	4.1141
59.5910	14.7725	12.0724	10.0002	7.5543	5.1500	3.9407
60.3061	16.1556	14.3870	13.4266	10.6878	7.2971	5.0911
60.4348	16.1846	14.4407	13.5369	10.8101	7.4704	5.3018
61.1506	14.4657	11.4873	9.4048	7.0517	5.0265	3.9722
61.8002	14.0471	10.9678	8.6018	6.1710	4.2880	3.3353
62.4112	14.1454	12.0060	10.6006	8.1658	5.7853	4.1182
62.4863	13.9818	11.8934	10.5702	8.2307	5.9479	4.3800
62.9980	11.3281	8.3922	5.9181	3.8068	2.4137	1.7614
63.5685	8.3869	5.6856	3.6944	2.2504	1.4409	1.0647
64.1272	6.2377	3.9644	2.3846	1.3611	0.8417	0.6076
64.6779	4.5836	2.7243	1.5061	0.8015	0.4675	0.3234
65.2240	3.3292	1.8500	0.9403	0.4678	0.2513	0.1623
65.7626	2.4193	1.2644	0.5965	0.2810	0.1358	0.0788
66.2978	1.7767	0.8833	0.3943	0.1797	0.0744	0.0385
66.8313	1.3339	0.6410	0.2775	0.1253	0.0488	0.0204
67.3627	1.0330	0.4877	0.2092	0.0951	0.0345	0.0117
67.8923	0.8275	0.3887	0.1674	0.0770	0.0270	0.0076
68.4205	0.6842	0.3221	0.1400	0.0651	0.0224	0.0055
68.9478	0.5812	0.2750	0.1206	0.0565	0.0193	0.0040
69.4741	0.5045	0.2400	0.1059	0.0499	0.0170	0.0030
70.0000	0.4452	0.2128	0.0944	0.0446	0.0150	0.0021
70.5249	0.3979	0.1909	0.0850	0.0403	0.0132	0.0015
71.0497	0.3593	0.1729	0.0772	0.0367	0.0116	0.0010

Table 2-2. Horizontal attenuation rates in dB/km at oxygen window frequencies (Ref 13: 78)

FREQ. (GHz)	Altitude, km 0	4	8	12	16	20
48.70	0.1795	0.0861	0.0383	0.0181	0.0050	0.0006
49.20	0.2061	0.0985	0.0437	0.0206	0.0068	0.0009
49.70	0.2390	0.1137	0.0502	0.0236	0.0080	0.0010
50.20	0.2811	0.1330	0.0583	0.0273	0.0093	0.0017
50.70	0.3363	0.1583	0.0688	0.0320	0.0110	0.0024
51.25	0.4204	0.1969	0.0846	0.0390	0.0134	0.0033
51.75	0.5297	0.2482	0.1056	0.0479	0.0165	0.0045
52.22	0.6766	0.3196	0.1354	0.0604	0.0211	0.00[illegible]
52.74	0.9139	0.4417	0.1885	0.0829	0.0295	0.00[illegible]
53.28	1.2835	0.6461	0.2834	0.1241	0.0454	0.0152
53.82	1.8307	0.9735	0.4481	0.1929	0.0750	0.0258
54.35	2.5992	1.4693	0.7186	0.3291	0.1279	0.0456
54.91	3.7293	2.2577	1.1852	0.5671	0.2248	0.0810
55.46	5.2343	3.3931	1.9095	0.9607	0.3853	0.1398
56.31	8.2337	6.4025	5.1248	3.7077	2.5633	1.7525
56.65	8.9620	6.5539	4.1902	2.3104	0.9344	0.3384
57.27	10.2805	7.5152	4.8060	2.6673	1.0662	0.3836
57.94	12.2242	9.2301	6.0261	3.4105	1.3354	0.4743
58.39	13.8498	12.1096	11.2256	8.9667	6.2491	4.0848
58.80	13.7710	10.5013	6.9529	4.0194	1.5601	0.5513
59.38	14.7076	12.1945	9.6572	6.4181	2.9598	1.1706
59.93	15.0075	11.5391	7.7245	4.5107	1.7547	0.6209
60.37	16.2152	14.5630	13.8896	11.2795	7.8640	5.0867
60.82	15.0167	11.5048	7.7480	4.4075	1.7236	0.6117
61.49	14.0210	10.4872	6.9049	3.9418	1.5735	0.5654
62.10	14.1369	10.9082	7.3622	4.2314	1.7153	0.6214
62.45	14.0728	11.9855	10.7032	8.3781	6.1434	4.5474
62.79	12.5507	9.6861	6.6799	3.9153	1.6705	0.6282
63.33	9.4799	6.4705	3.8497	2.0239	0.8184	0.2982
63.90	7.0340	4.5018	2.5153	1.2613	0.5091	0.1857
64.44	5.2404	3.1560	1.6504	0.7887	0.3118	0.1122
65.00	3.7960	2.1404	1.0450	0.4788	0.1853	0.0657
65.54	2.7578	1.4636	0.6731	0.2993	0.1126	0.0391
66.09	1.9982	1.0050	0.4412	0.1938	0.0708	0.0239
66.64	1.4733	0.7126	0.3049	0.1347	0.0479	0.0155
67.16	1.1343	0.5371	0.2283	0.1024	0.0357	0.0104
67.70	0.8934	0.4195	0.1795	0.0819	0.0283	0.0080
68.68	0.6296	0.2970	0.1296	0.0605	0.0207	0.0048
69.21	0.5404	0.2564	0.1128	0.0530	0.0180	0.0032
69.73	0.4738	0.2260	0.1000	0.0472	0.0159	0.0028
70.26	0.4205	0.2014	0.0895	0.0424	0.0139	0.0020
70.78	0.3783	0.1817	0.0811	0.0385	0.0122	0.0014

during heavy rainfall and severe attenuation during moderate rainfall. This constraint must be understood and accounted for in any communication system design using millimeter waves.

The first theoretical study of attenuation of very short waves was made by Ryde during the second world war. Since then, theoretical attempts to predict the attenuation due to rain were made many times. These initial investigations revealed little agreement with the experimental work. In the early seventies, Robert K. Crane produced results in a simulated rainfall which agreed well with the theoretical calculations. It is now generally accepted that the poor comparison of early efforts was due to a combination of inadequate rain rate sampling and lack of spatial rain uniformity (Reference 10: 321).

One goal of rain attenuation studies is to provide useful information for communication system design, including accurate estimates of the excess attenuation caused by rain. From such studies, prediction models may be developed. With this in mind, the following (Reference 8: 1465) have been identified as being desirable features of a prediction model:

1. Simple. Applications to communication system design should avoid mathematical complexity and should be straight forward.

2. Physically sound. The model should closely agree with directly observed physical data such as spatial rain behavior.

3. Data tested. The model should be checked against measured data from many different regions. Emphasis should be given to the data at low percentages of time that are of most interest to system designers.

4. Flexible. The model should be able to accept modifications. As more and better data becomes available, refinements are likely to be required.

Today, a number of rain attenuation prediction models are available. They may be classified as using either an empirical approach, a rain-cell approach, or a rain-profile approach (Reference 8: 1466). The primary difference in these methods is the way they treat the rain rate along a radio path. If the rain rate were uniform over a path of length L, then the rain attenuation (dB) due to rain would simply be the attenuation (dB/km) multiplied by the path length (km). However, actual rainfalls are typically non-uniform. These approaches are based on the relationship between attenuation and rain rate which is approximated by:

$$A = aR^b \qquad (2.4)$$

where

A = specific attenuation (dB/km).
R = rain rate (mm/hr).
a, b = empirical constants.

Roderic L. Olsen, et al. (Reference 9) has proven this empirical relationship to be a reasonably accurate approximation to a more general theoretical relation. In his paper, Olsen presented a set of precise values for a and b for 41 frequencies between 1 and 1000 GHz. The parameters a and b depend on the millimeter wave frequency and the shape, size, and temperature of the rain drops. Values for a and b are given in tabular (Tables II-4, II-5, and II-6) and graphical (Figures II-4 and II-5) form for the drop size distribution of Laws and Parsons,

Table II-4. Regression calculations for a and b as functions of frequency and drop size distribution. Rain temperature = 0°C (Ref 9: 323).

FREQ (GHz)	a					b				
	LP_L	LP_H	MP	J-T	J-D	LP_L	LP_H	MP	J-T	J-D
1.0	6.61x10^{-5}	5.25x10^{-5}	8.60x10^{-5}	4.71x10^{-5}	8.63x10^{-5}	0.991	0.947	0.853	0.899	0.843
1.5	1.45x10^{-4}	1.16x10^{-4}	1.93x10^{-4}	9.31x10^{-5}	1.96x10^{-4}	0.988	0.976	0.870	0.967	0.847
2.0	2.61x10^{-4}	1.98x10^{-4}	3.45x10^{-4}	1.36x10^{-4}	3.47x10^{-4}	0.930	1.012	0.891	1.049	0.851
2.5	4.16x10^{-4}	2.98x10^{-4}	5.46x10^{-4}	1.63x10^{-4}	5.48x10^{-4}	0.955	1.054	0.917	1.208	0.857
3.0	6.15x10^{-4}	4.12x10^{-4}	7.99x10^{-4}	2.09x10^{-4}	8.01x10^{-4}	0.984	1.108	0.947	1.353	0.864
3.5	8.61x10^{-4}	5.62x10^{-4}	1.11x10^{-3}	3.38x10^{-4}	1.11x10^{-3}	1.015	1.150	0.981	1.351	0.871
4.0	1.16x10^{-3}	6.86x10^{-4}	1.47x10^{-3}	5.38x10^{-4}	1.48x10^{-3}	1.049	1.202	1.016	1.350	0.879
5.0	1.96x10^{-3}	1.12x10^{-3}	2.41x10^{-3}	1.38x10^{-3}	2.40x10^{-3}	1.113	1.274	1.079	1.288	0.896
6.0	3.35x10^{-3}	1.99x10^{-3}	3.71x10^{-3}	3.08x10^{-3}	3.59x10^{-3}	1.156	1.295	1.126	1.221	0.913
7.0	4.55x10^{-3}	3.38x10^{-3}	5.44x10^{-3}	5.57x10^{-3}	5.07x10^{-3}	1.188	1.270	1.167	1.167	0.929
8.0	6.49x10^{-3}	5.35x10^{-3}	7.65x10^{-3}	9.07x10^{-3}	6.86x10^{-3}	1.187	1.245	1.156	1.118	0.943
9.0	8.88x10^{-3}	8.03x10^{-3}	1.08x10^{-2}	1.29x10^{-2}	8.98x10^{-3}	1.195	1.216	1.155	1.091	0.957
10	1.17x10^{-2}	1.14x10^{-2}	1.36x10^{-2}	1.69x10^{-2}	1.14x10^{-2}	1.178	1.189	1.150	1.076	0.968
11	1.51x10^{-2}	1.52x10^{-2}	1.73x10^{-2}	2.12x10^{-2}	1.41x10^{-2}	1.171	1.167	1.143	1.065	0.977
12	1.86x10^{-2}	1.96x10^{-2}	2.15x10^{-2}	2.62x10^{-2}	1.72x10^{-2}	1.162	1.150	1.138	1.052	0.985
15	3.21x10^{-2}	3.47x10^{-2}	3.68x10^{-2}	4.66x10^{-2}	2.82x10^{-2}	1.142	1.119	1.118	1.018	1.003
20	6.29x10^{-2}	7.09x10^{-2}	7.19x10^{-2}	9.83x10^{-2}	5.30x10^{-2}	1.119	1.083	1.097	0.966	1.020
25	0.105	0.132	0.121	0.173	0.101	1.096	1.059	1.076	0.956	1.033
30	0.162	0.226	0.186	0.276	0.170	1.081	0.984	1.063	0.823	1.044
35	0.232	0.345	0.268	0.372	0.288	1.072	0.907	1.057	0.783	1.053
40	0.313	0.467	0.362	0.451	0.261	0.881	0.844	0.972	0.760	1.058
50	0.489	0.669	0.570	0.629	0.307	0.907	0.815	0.995	0.709	1.063
60	0.658	0.796	0.801	0.808	0.558	0.950	0.796	0.951	0.662	1.035
70	0.801	0.869	1.00	0.933	0.760	0.809	0.780	0.812	0.661	1.009
80	0.924	0.913	1.19	0.809	0.922	0.778	0.780	0.781	0.674	0.980
90	1.02	0.945	1.35	0.857	1.10	0.756	0.776	0.753	0.663	0.953
100	1.08	0.966	1.48	0.961	1.26	0.742	0.774	0.730	0.637	0.928
110	1.12	0.979	1.59	1.08	1.41	0.736	0.771	0.716	0.616	0.906
120	1.15	0.981	1.67	1.10	1.55	0.727	0.771	0.702	0.604	0.882
150	1.25	0.993	1.88	1.09	1.89	0.703	0.769	0.677	0.610	0.829
200	1.36	1.05	2.06	1.01	2.33	0.668	0.764	0.640	0.612	0.773
250	1.49	1.08	2.13	0.983	2.60	0.660	0.763	0.636	0.614	0.724
300	1.44	1.00	2.24	0.976	2.78	0.661	0.764	0.638	0.611	0.692
350	1.44	0.950	2.23	0.988	2.87	0.659	0.765	0.638	0.609	0.673
400	1.40	0.909	2.19	0.991	2.92	0.660	0.766	0.641	0.610	0.664
500	1.33	0.930	2.14	0.994	2.94	0.666	0.767	0.641	0.609	0.650
600	1.28	0.902	2.11	0.999	2.95	0.669	0.768	0.609	0.608	0.630
700	1.25	0.884	2.08	0.991	2.96	0.671	0.769	0.638	0.638	0.620
800	1.22	0.868	2.05	0.984	2.94	0.672	0.770	0.638	0.611	0.616
900	1.21	0.858	2.03	0.969	2.91	0.673	0.770	0.638	0.613	0.614
1000	1.19	0.850	2.00	0.956	2.89	0.674	0.771	0.638	0.615	0.612

* See footnote 2 regarding modified values of a and b for MP, J-T, and J-D distributions.

Marshall and Palmer, and Joss et al. These values were computed by applying logarithmic regression to scattering calculations. To obtain greater accuracy, two regressions were performed for the Laws and Parsons drop size distribution: one at "low" rain rate designated LP_L and one at "high" rain rates designated LP_H. The Marshall and Palmer drop size distribution is designated MP. The drop size distribution of Joss et al. are designated J-T for the "thunderstorm" distribution and J-D for the "drizzle" distribution. The Laws and Parsons distribution is preferred due to the tendency of the others to overestimate attenuation at the higher frequencies (Reference 8: 1466). The values are given for three different temperatures. The values for -10°C and +20°C give reasonable bounds. For most climates, the 0°C rain temper-

Table II-5. Regression calculations for a and b as functions of frequency and drop size distribution. Rain temperature = 20°C (Ref 9: 323).

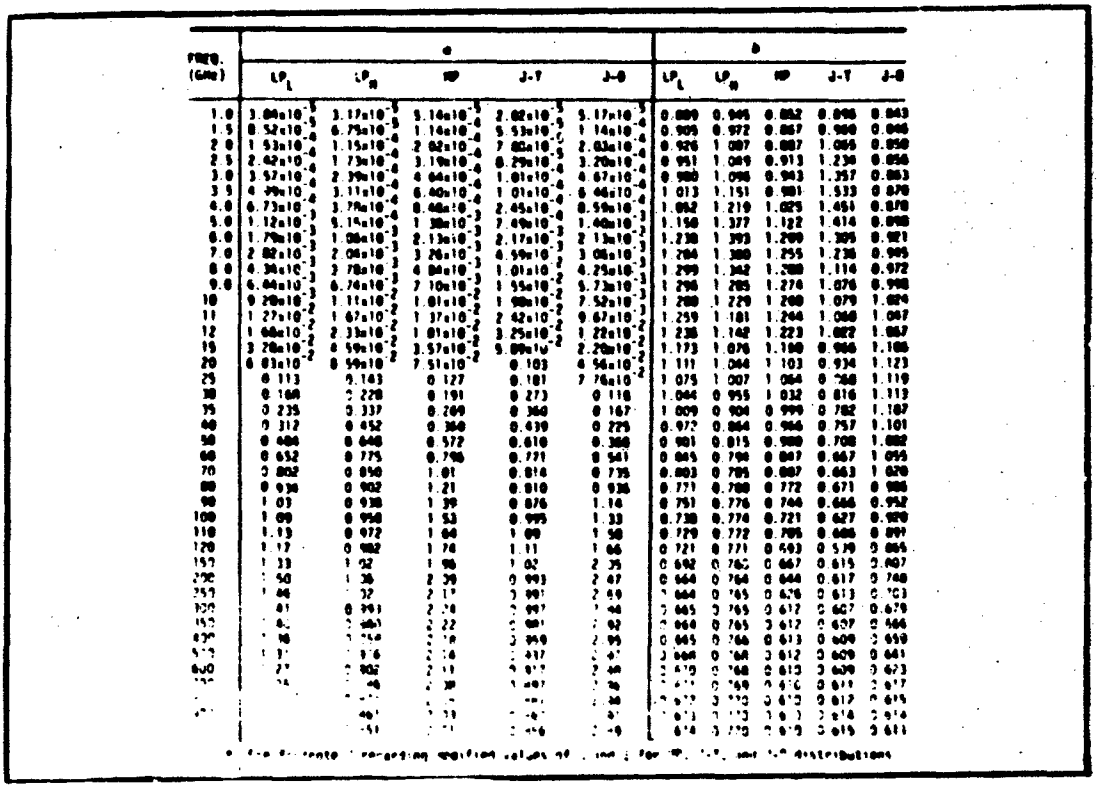

ature will give values to be expected (Reference 9: 322). The values are for spherical raindrops even though actual raindrops are distorted. For most applications above 10 GHz, the spherical model for raindrops is adequate (Reference 8: 1466).

On the basis of using the 0°C rain temperature, the drop size distribution of Laws and Parsons, and spherical rain drops to obtain reasonable values of specific attenuation. The following equations (Reference 8: 1467) are a convenient source for computing the coefficients a and b for any frequency of interest.

$$a(f) = (4.21 \times 10^{-5}) f^{2.42} \qquad 2.9 \leq f \leq 54 \text{ GHz} \qquad (2.5)$$

$$a(f) = (4.09 \times 10^{-2}) f^{0.699} \qquad 54 \leq f \leq 180 \text{ GHz} \qquad (2.6)$$

$$b(f) = (1.41)f^{-0.0799} \qquad 8.5 \leq f \leq 25 \text{ GHz} \qquad (2.7)$$

$$b(f) = (2.63)f^{-0.272} \qquad 25 \leq f \leq 164 \text{ GHz} \qquad (2.8)$$

Should more precise values of a and b be desired, the tabulated values should be used.

Table II-6. Regression calculations for a and b as functions of frequency and drop size distribution. Rain temperature = -10°C (Ref 9: 324).

FREQ (GHz)	a					b				
	LP_L	LP_M	MP	J-T	J-E	LP_L	LP_M	MP	J-T	J-E
1.0	8.68×10^{-5}	7.13×10^{-5}	1.16×10^{-4}	6.35×10^{-5}	1.17×10^{-4}	0.890	0.948	0.894	0.90[illegible]	0.843
1.5	1.97×10^{-4}	1.55×10^{-4}	2.62×10^{-4}	1.26×10^{-4}	2.63×10^{-4}	0.905	0.978	0.871	0.97[illegible]	0.84[illegible]
2.0	3.55×10^{-4}	2.67×10^{-4}	4.71×10^{-4}	1.89×10^{-4}	4.72×10^{-4}	0.931	1.014	0.892	1.065	0.852
2.5	5.62×10^{-4}	4.05×10^{-4}	7.45×10^{-4}	2.48×10^{-4}	7.47×10^{-4}	0.955	1.053	0.917	1.109	0.856
3.0	8.34×10^{-4}	5.68×10^{-4}	1.09×10^{-3}	3.39×10^{-4}	1.09×10^{-3}	0.981	1.094	0.944	1.243	0.864
3.5	1.17×10^{-3}	7.57×10^{-4}	1.51×10^{-3}	5.06×10^{-4}	1.51×10^{-3}	1.008	1.134	0.971	1.271	0.872
4.0	1.57×10^{-3}	9.80×10^{-4}	2.00×10^{-3}	7.81×10^{-4}	2.00×10^{-3}	1.033	1.171	0.998	1.270	0.877
5.0	2.59×10^{-3}	1.62×10^{-3}	3.26×10^{-3}	1.79×10^{-3}	3.22×10^{-3}	1.077	1.214	1.041	1.228	0.889
6.0	3.96×10^{-3}	2.66×10^{-3}	4.91×10^{-3}	3.45×10^{-3}	4.76×10^{-3}	1.105	1.222	1.068	1.180	0.901
7.0	5.70×10^{-3}	4.14×10^{-3}	6.98×10^{-3}	5.68×10^{-3}	6.63×10^{-3}	1.119	1.214	1.083	1.145	0.910
8.0	7.81×10^{-3}	6.07×10^{-3}	9.50×10^{-3}	8.43×10^{-3}	8.82×10^{-3}	1.125	1.199	1.090	1.118	0.919
9.0	1.03×10^{-2}	8.46×10^{-3}	1.25×10^{-2}	1.16×10^{-2}	1.16×10^{-2}	1.126	1.185	1.092	1.099	0.926
10	1.32×10^{-2}	1.13×10^{-2}	1.59×10^{-2}	1.51×10^{-2}	1.47×10^{-2}	1.125	1.171	1.092	1.087	0.932
11	1.64×10^{-2}	1.45×10^{-2}	1.97×10^{-2}	1.91×10^{-2}	1.74×10^{-2}	1.124	1.161	1.091	1.077	0.938
12	2.00×10^{-2}	1.81×10^{-2}	2.39×10^{-2}	2.37×10^{-2}	2.09×10^{-2}	1.122	1.152	1.090	1.066	0.942
15	3.31×10^{-2}	3.14×10^{-2}	3.94×10^{-2}	4.23×10^{-2}	3.34×10^{-2}	1.119	1.135	1.086	1.027	0.954
20	6.37×10^{-2}	6.68×10^{-2}	7.50×10^{-2}	9.73×10^{-2}	6.09×10^{-2}	1.111	1.096	1.082	0.95[illegible]	0.97[illegible]
25	0.107	0.130	0.126	0.174	9.73×10^{-2}	1.091	1.037	1.065	0.87[illegible]	0.966
30	0.165	0.226	0.193	0.276	0.143	1.055	0.969	1.037	0.826	1.004
35	0.236	0.346	0.275	0.376	0.197	1.021	0.910	1.002	0.784	1.016
40	0.316	0.468	0.370	0.455	0.260	0.981	0.857	0.966	0.761	1.025
50	0.487	0.665	0.579	0.619	0.404	0.910	0.819	0.904	0.714	1.027
60	0.645	0.789	0.787	0.800	0.564	0.856	0.796	0.854	0.684	1.016
70	0.777	0.860	0.973	0.840	0.728	0.817	0.795	0.817	0.659	0.997
80	0.888	0.903	1.14	0.809	0.888	0.787	0.781	0.789	0.673	0.974
90	0.980	0.935	1.26	0.834	1.04	0.765	0.777	0.764	0.668	0.953
100	1.05	0.957	1.41	0.920	1.18	0.749	0.771	0.741	0.646	0.933
110	1.09	0.974	1.51	1.01	1.32	0.739	0.771	0.726	0.624	0.[illegible]14
120	1.12	0.980	1.59	1.06	1.44	0.733	0.770	0.712	0.611	0.896
150	1.20	0.979	1.80	1.05	1.76	0.711	0.769	0.686	0.610	0.846
200	1.42	1.03	2.04	1.02	2.21	0.674	0.765	0.652	0.609	0.[illegible]14
250	1.56	1.04	2.11	1.01	2.53	0.659	0.763	0.636	0.606	0.739
300	1.65	1.01	2.22	0.972	2.72	0.660	0.764	0.618	0.612	0.704
350	1.65	0.994	2.23	0.963	2.82	0.656	0.764	0.617	0.610	0.684
400	1.62	0.976	2.19	0.942	2.88	0.658	0.765	0.611	0.612	0.669
500	1.54	0.936	2.14	0.927	2.91	0.664	0.767	0.611	0.611	0.655
600	1.29	0.904	2.11	0.919	2.94	0.669	0.769	0.609	0.609	0.634
700	1.25	0.883	2.08	0.903	2.95	0.671	0.769	0.609	0.609	0.622
800	1.22	0.869	2.05	0.888	2.93	0.672	0.770	0.610	0.611	0.617
900	1.21	0.857	2.03	0.87[illegible]	2.91	0.673	0.770	0.610	0.613	0.614
1000	1.19	0.849	2.01	0.85[illegible]	2.89	0.674	0.771	0.611	0.614	0.612

* See footnote 2 regarding modified values of [illegible] and [illegible] for MP, J-T, and J-E distributions

C. Fog and Clouds. Some typical attenuation values for fog, water clouds, and ice clouds as a function of frequency and temperature are shown in Figure II-6. Generally, cloud attenuation rates depend on the liquid water content. The attenuation of cirrus ice clouds is negligible (Reference 4: 39-40).

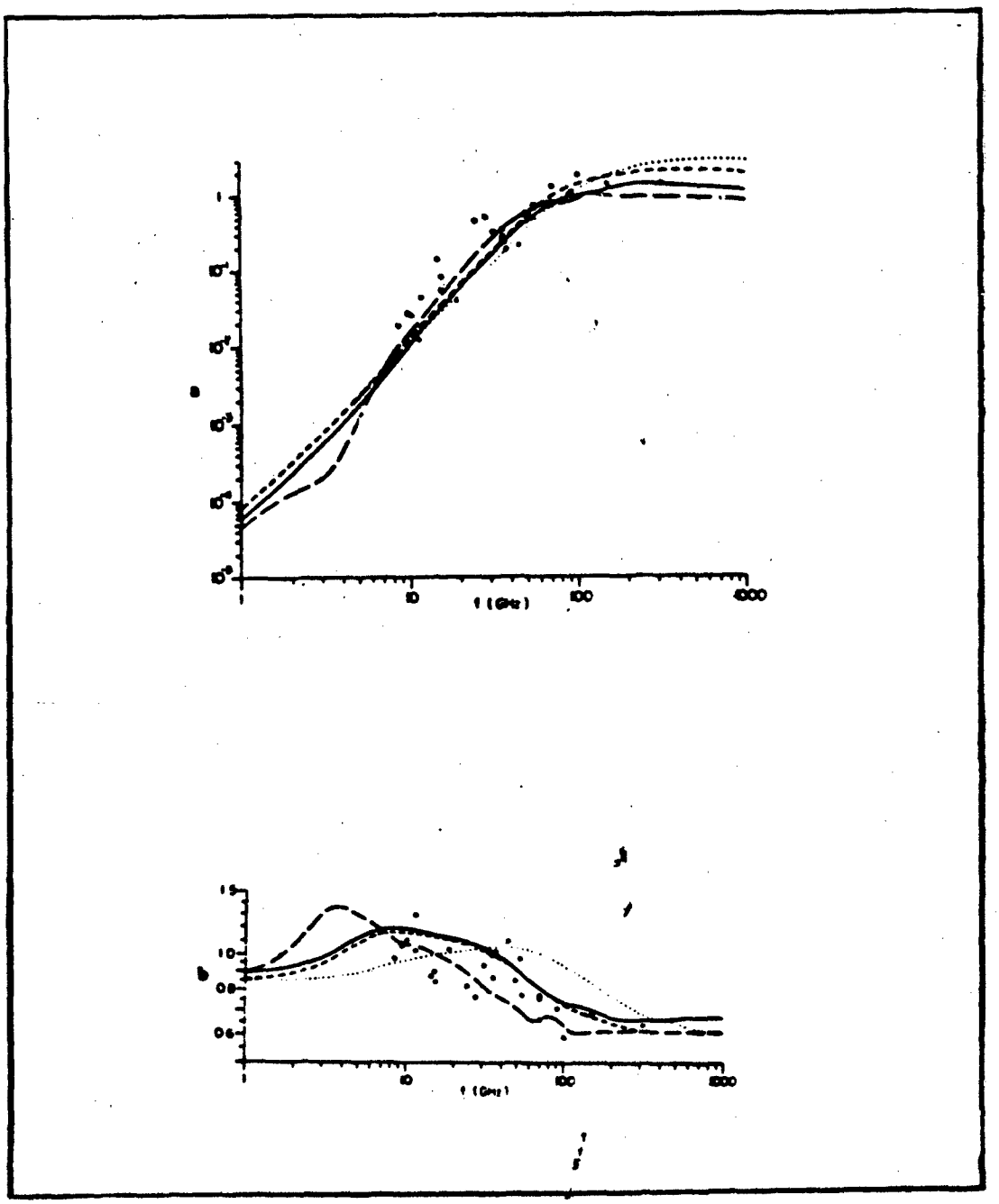

Fig II-4. (a) Dependence of a on frequency and drop size distribution for a rain temperature of 0°C. —— LP distribution; --- MP distribution; — — — J-T distribution; ···· J-D distribution; • Experimental values. (b) Dependence of b on frequency and drop size distribution for a rain temperature of 0°C. (Ref 9: 324).

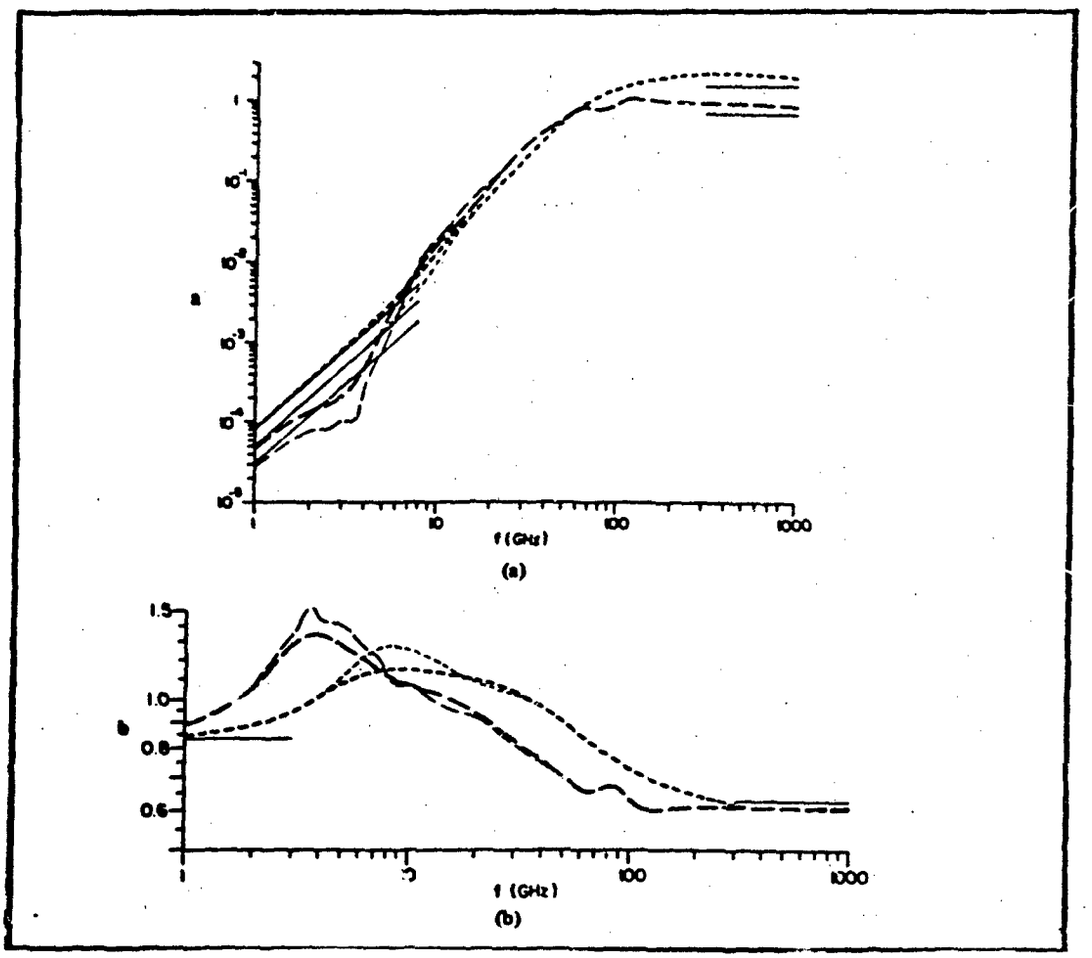

Fig II-5. (a) Dependence of a on frequency and rain temperature. MP distribution: --- 0°C, --- 20°C; J-T distribution: —— 0°C, —— 20°C; low and high frequency asymptotes: ——. (b) Dependence of b on frequency and rain temperature. MP distribution: --- 0°C, --- 20°C; J-T distribution: —— 0°C, —— 20°C; low and high frequency asymptotes: —— (Reference 9: 325).

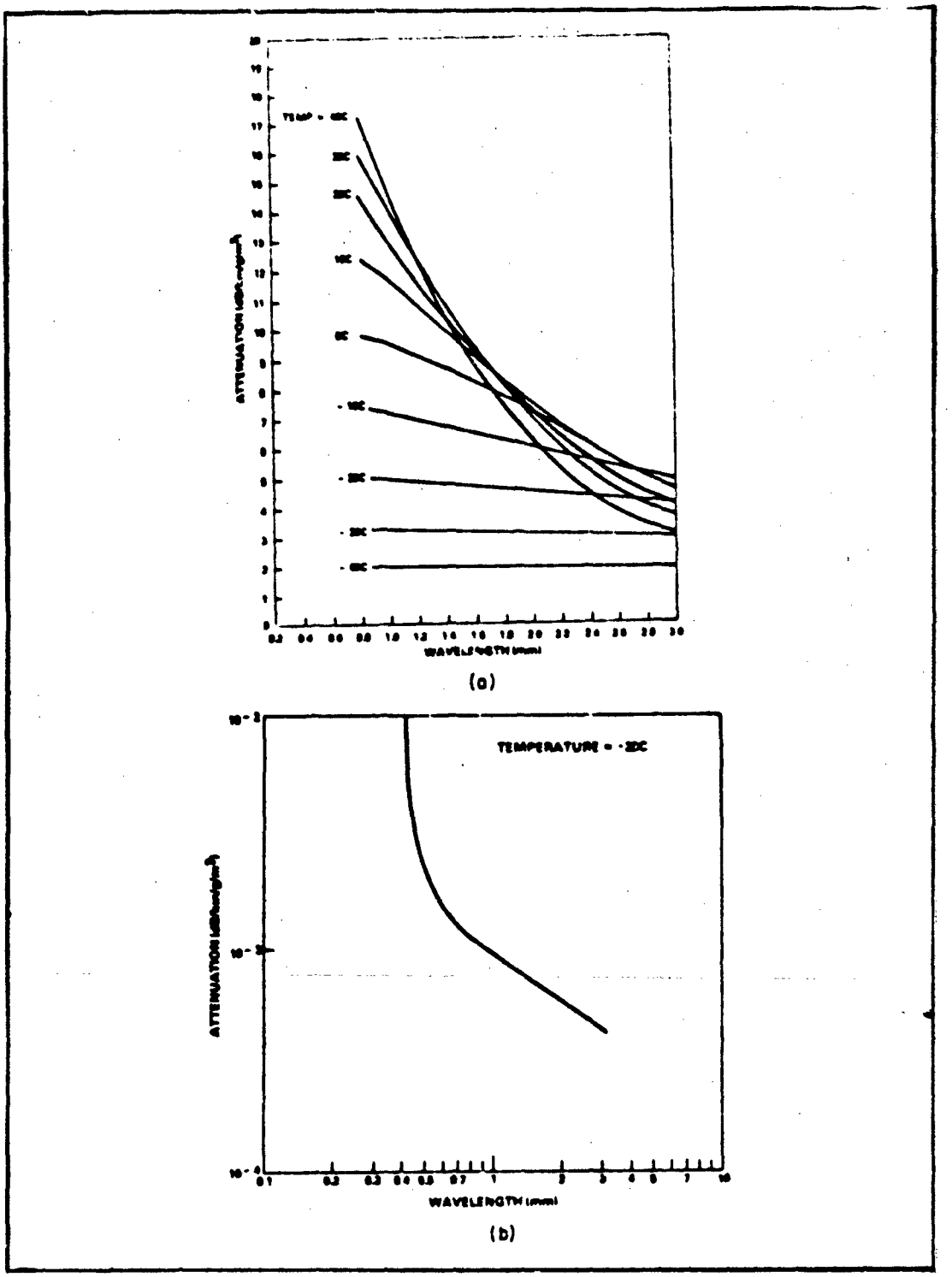

Fig II-6. Fog and cloud attenuation properties. (a) Cloud and fog attenuation, (b) ice cloud or fog attenuation (Ref 4:39).

c. Smoke and Dust. Attenuation of millimeter waves due to smoke and dust is of particular interest for military applications. In October 1978, the Atmospheric Sciences Laboratories conducted a major test called DIRT-I, to obtain direct sensor information about the properties of dust produced by battlefield explosions (Reference 15: 11). Measurements varied, sometimes reaching 30 dB with durations lasting up to 20 seconds. The large attenuations were caused by large pieces of soil blown in the air. The residual dust remaining in the air made no significant contribution (Reference 18: 103). A rough rule-of-thumb is to add 1 dB of total attenuation for each gram per square centimeter of path integrated dust for a 100 GHz wave (Reference 2: 114).

2. Fading

The principal reason for fading of radio signals is the interference of the direct wave and the waves reflected from the inhomogenities of the troposphere. The multipath interference pattern constantly shifts as the various atmospheric variables, primarily pressure, temperature, and water vapor content change. Because the air masses with refractive index higher or lower than average are constantly moving, the refractive effect is very small. Fade depth increases with signal frequency and path length. Fading usually consists of slow, low amplitude variations superimposed upon faster and larger ones. Maximum fades are on the order of less than one dB per nautical mile of path length in the 30 to 60 GHz region. So substantial path lengths are required before fading becomes a problem. It should be noted that specular reflection and ducting are of much less importance at

millimeter wavelengths than at lower frequencies because the reflecting surface roughness is greater relative to the wavelength (Reference 12: 52-53).

Calculation of a Communication Link

The propagation conditions previously discussed must lead to numerical results if they are to be of any use to a communication design. Millimeter wave transmissions are best described by the power received at the input of the receiver. The received power is calculated by inter-relating the radiated power, antenna gain, and transmission losses. Radiated power depends on the antenna's efficiency. Typical values for the efficiency of a parabolic antenna range between 0.50 and 0.60. Antenna efficiency is usually included in the antenna's specifications which are supplied by the manufacturer. Antenna gains may be computed using established equations. Transmission losses are in the form of tables, graphs, or formulas.

The communication link equation is derived by taking the Friis equation (Reference 21: 29) and accounting for tropospheric absorbtion loss. In terms of decibels, the link equation has the form:

$$P_r(dBm) = P_t(dBm) + G_t(dB) + G_r(dB) - L_s(dB) \qquad (2.9)$$

$$L_s(dB) = L_b(dB) + L_t(dB) + L_g(dB) + L_d(dB) + L_f(dB) \qquad (2.10)$$

where

P_r = Received power level at receiver/antenna junction

P_t = Transmitted power level at transmitter/antenna

G_t = Transmit antenna gain

Table II-7. Communication link equations
(Reference 2: 69).

Friis Equation: $$P_r = P_t \frac{A_t A_r}{\lambda^2 R^2}, \qquad (2.11)$$

$$G = \frac{4\pi}{\lambda^2} A; \qquad A = G \frac{\lambda^2}{4\pi}; \qquad A = A_g \times \eta.$$

$$P_r = P_t G_t \frac{\lambda}{4\pi} \times G_r \frac{\lambda^2}{4\pi} \times \frac{1}{\lambda^2 R^2}.$$

$$P_r = P_t G_t G_r \frac{\lambda^2}{(4\pi R)^2}; \qquad P_r \text{ (dBW)} = 10 \log_{10} (P_r). \qquad (2.12)$$

Taking tropospheric absorbtion loss (L_t) into account:

$$P_r = P_t G_t G_r \frac{\lambda^2}{(4\pi R)^2} \times \frac{1}{L_t}. \qquad (2.13)$$

where

P_r = Received power level at receiver/antenna junction

P_t = Transmitted power level at transmitter/antenna junction

A_t and A_r = The respective transmit and receive effective antenna aperatures

A_g = Geometric antenna aperature in meters squared

η = Antenna radiation efficiency (typically 0.50 to 0.80)

λ = Wavelength in meters

R = Range in meters

L_b = Basic free space loss = $\lambda^2/(4\pi R)^2$

L_t = Tropospheric absorbtion loss

Table II-8. Antenna gain and beamwidth equations (Reference 2: 70).

For antennas in general:

$$G = \frac{4\pi}{\lambda^2} A; \quad A = A_g \times \eta; \quad \lambda = \frac{c}{f}.$$

For a parabolic antenna:

$$A = \pi r^2 \times \eta; \qquad G = \frac{(2\pi r)^2}{\lambda^2} \eta,$$

$$G = \frac{(\pi D)^2}{\lambda^2} \eta; \qquad G\ (dB) = 10 \log_{10} (G). \tag{2.14}$$

$$BW = \frac{70\lambda}{D}, \text{ for millimeter wave frequencies} \tag{2.15}$$

where

G = Antenna gain

λ = Wavelength in meters

c = Speed of light = 3.0×10^8 meters/second

f = Frequency in Hertz

A = Effective antenna aperature in meters squared

A_g = Geometric antenna aperature

η = Antenna radiation efficiency (0.50 to 0.60 for parabolic antennas)

r = Antenna radius in meters

D = Antenna diameter in meters

BW = Half-power antenna beamwidth

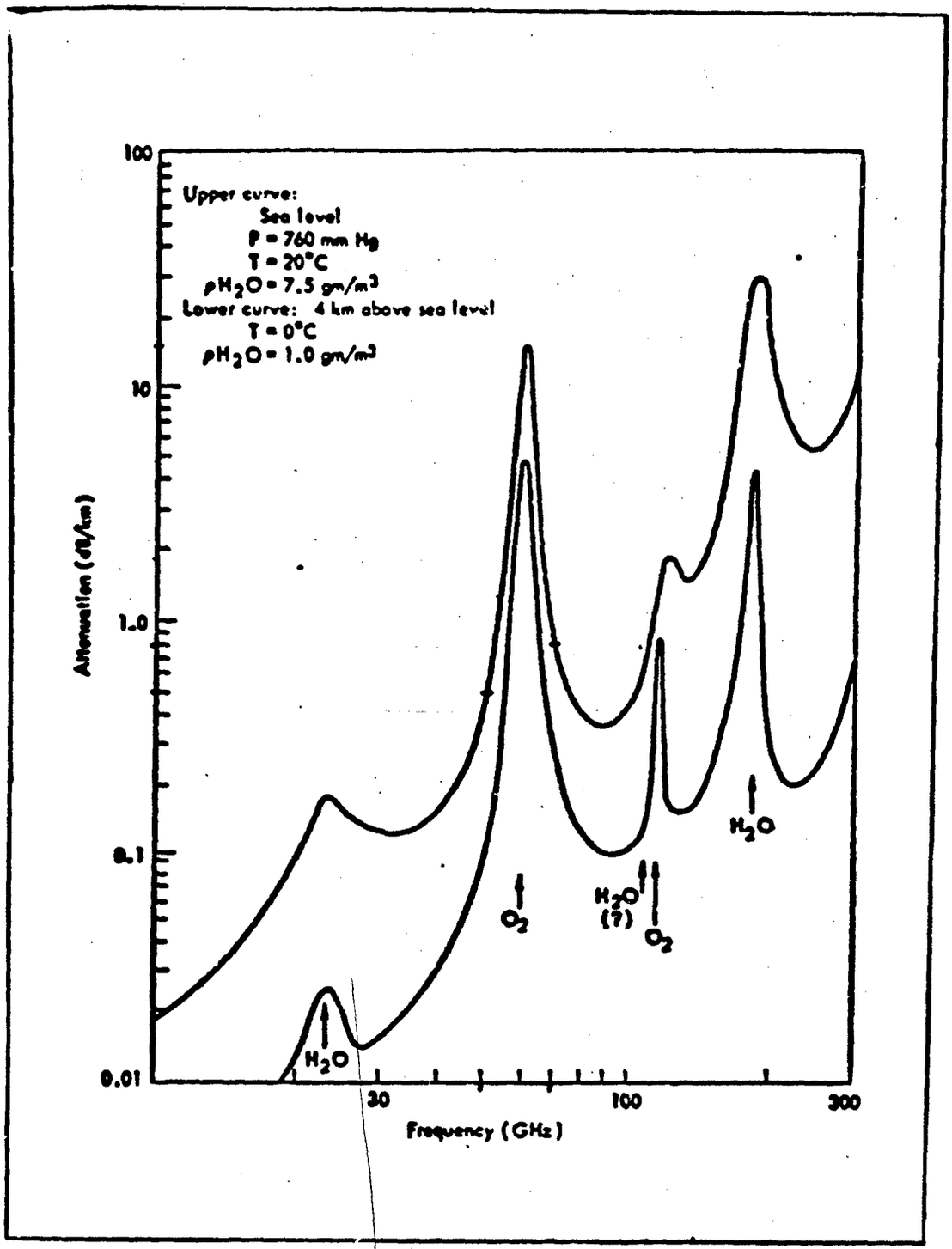

Figure II-7. Horizontal tropospheric absorbtion attenuation (Reference 2: 71).

G_r = Receive antenna gain

L_s = Total transmission loss

L_b = Basic free space loss

L_t = Tropospheric absorbtion loss

L_g = Ground reflected multipath loss

L_d = Diffraction loss

L_f = Atmospheric fading loss.

Since tropospheric absorbtion loss is so predominant in comparison with losses due to the last three terms, they may be disregarded in first order considerations.

Example

In order to gain a better understanding of the high tropospheric absorbtion and the short operation range of millimeter waves, it is instructional to go through an example. Assume identical transceivers at each end of the link. Each is equipped with a four-inch (D = 0.1016m) parabolic antenna. For sake of simplicity, a typical receiver sensitivity of -89.0 dBm is assumed for voice transmissions.

Let

$$P_t = 100 \text{ milliwatts (20 dBm)} \tag{2.16}$$

$$R = 2.5 \text{ kilometers } (2.5 \times 10\text{m}). \tag{2.17}$$

Using equation 2.14 of Table II-8: $\eta = 0.55$:

$$G_t = G_r = 2{,}241 \text{ (33.5 dBm)}. \tag{2.18}$$

Using equation 2.15 of Table II-8:

$$\text{Beamwidth} = 3.4 \text{ degrees}. \tag{2.19}$$

From Table II-7:

$$L_b = 2.533 \times 10^{-14} \quad (-136 \text{ dB}). \tag{2.20}$$

Using Figure II-7 for 60 GHz:

$$L_t = 2.5 \text{ km} \times 16 \text{ dB/km} = 40 \text{ dB loss}. \tag{2.21}$$

Thus, using the equation for P_r:

$$\begin{aligned} P_r &= 20 \text{ dBm} + 33.5 \text{ dBm} + 33.5 \text{ dBm} - 136 \text{ db} - 40 \text{ dB} \\ &= -89.0 \text{ dBm}. \end{aligned} \tag{2.22}$$

This example illustrates the limited range of the 60 GHz absorbtion band in clear weather. Repeating this example for different ranges at 60 GHz illustrates the change in P_r. Figure II-8 summarizes this example. A comparison with 50 GHz and 70 GHz is included in Figure II-8 to demonstrate the substantial increase in operating range of frequencies with reduced tropospheric absorbtion.

In order to find the signal-to-noise ratio, the noise level must be found. The noise power level is calculated (Reference 20: 487) from:

$$P_{int} = G_a K T_e \tag{2.23}$$

where

P_{int} = Receiv. output noise power due to internal noise

G_a = Available gain of receiver

T_e = Receiver noise temperature

B = System bandwidth

K = Boltzman constant, 1.38×10^{-23}

Equation (23) is written in terms of decibels as:

$$P_{int}\ 10 \log_{10} G_a + 10 \log_{10} K + 10 \log_{10} T_e + 10 \log_{10} B \qquad (2.24)$$

Since both the signal and noise are multiplied by the same gain, receiver gain may be considered unity. Re-arranging equation (24) into a more common form:

$$P_{int} = 10 \log_{10}(K T_o) + 10 \log_{10}\left(\frac{T_e}{T_o}\right) + 10 \log_{10} B \qquad (2.25)$$

where $T_o = 290$ K is room temperature. For most systems other than earth-space links, $T_e = T_o$. Thus,

$$P_{int} = -174 \text{ dBm} + 10 \log_{10} B. \qquad (2.26)$$

Hence, the signal-to-noise ratio at the receiver output is

$$(SNR_o)_{dB} = P_r - P_{int}. \qquad (2.27)$$

For our original example with a bandwidth of 50 MHz,

$$(SNR_o)_{dB} = -89 \text{ dBm} + 174 \text{ dBm} - 10 \log_{10} (50 \times 10^6) \text{ dBm}$$
$$= 8 \text{ dBm}. \qquad (2.28)$$

For a bandwidth of 25 MHz,

$$(SNR_o)_{dB} = 11 \text{ dBm}. \qquad (2.29)$$

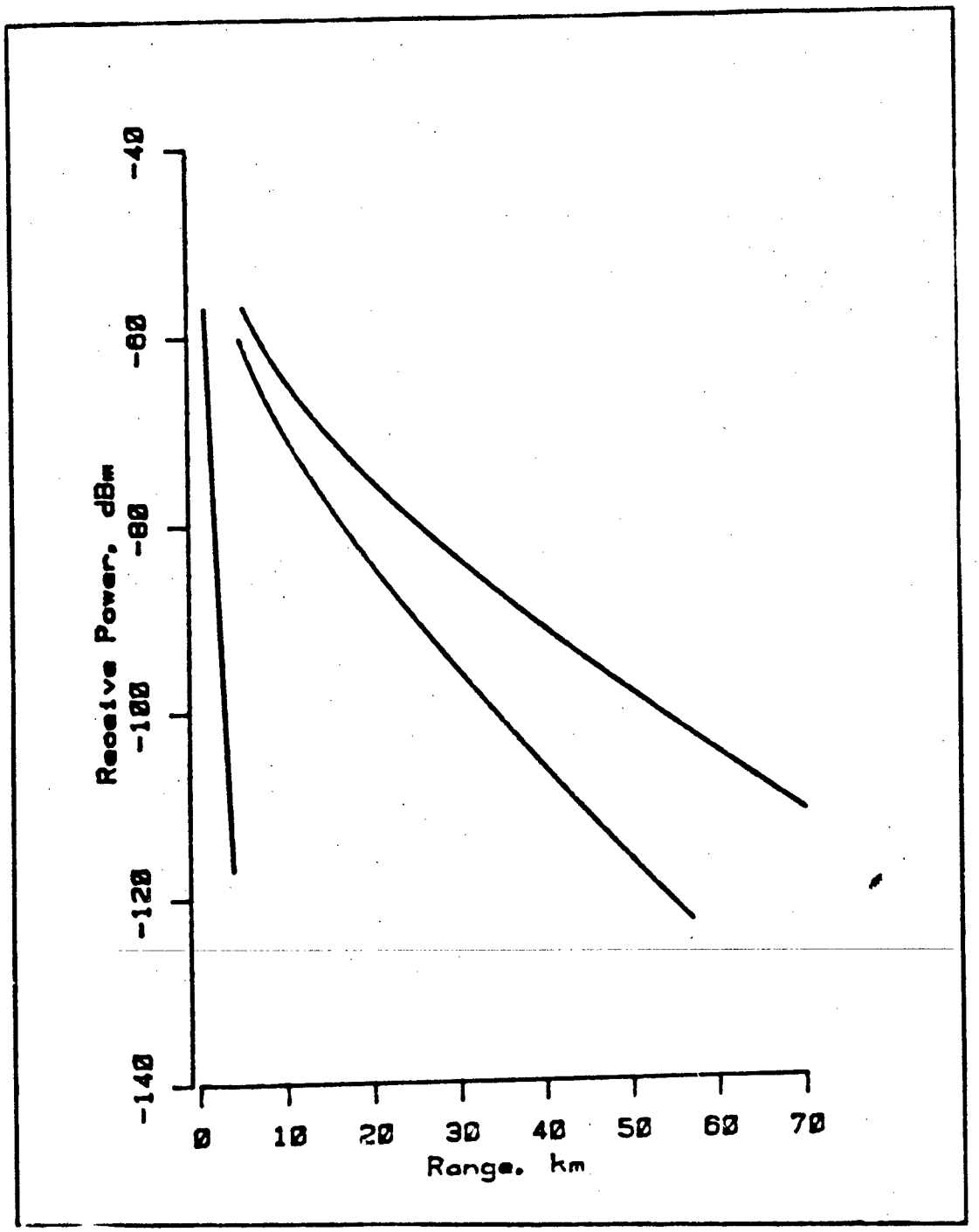

Fig II-8. Range example illustrating the substantial operating range of frequencies with reduced tropospheric absorbtion.

Chapter 3: Description of the Simulated Link Equations

Introduction

This chapter presents an overview of the Pascal-coded software developed in order to assess the relative data transmission performance of various modulation methods at millimeter wavelengths. This is done with and without jamming. Briefly, modulation is the process of impressing an information signal onto a carrier. All types of modulation methods may be used in transmitting digital data. The various methods may be used in transmitting digital data. The various methods differ in relative performance, flexibility, and complexity. The error rate in the presence of an additive white Guassian noise (AWGN) environment for a fixed data rate provides a good measure of data transmission performance. The specific digital modulation schemes incorporated in the computer program required exact analytical expressions for bit error probability in an AWGN channel be avaiable. For this reason, the modulation techniques used were binary orthogonal signaling which includes coherent binary frequency-shift keying (FSK) and coherent binary amplitude-shift keying (ASK), binary antipodal signaling which includes coherent binary phase-shift keying (PSK), non-coherent binary ASK and FSK, binary differentially encoded phase-shift keying (DPSK), and quadrature phase-shift keying (QPSK). The overview consists of a brief description of the input parameters, the calculation of the received power level, the calculation of the signal-to-noise ratio, and the calculation of the bit error rate for a particular modulation technique. First, a description of the basic scenario is presented.

Basic Scenario

In order to evaluate jamming effects on millimeter waves, the non-jammed digital communication link must first be presented to serve as a basis for comparisons. The model is simple, consisting only of a transmitter and a receiver. The transmitter/receiver arrangement is assumed to lay on a line-of-sight path free from the effects of multipath transmission. Such an arrangement may be thought of as existing on two airborne platforms. The distance between the transmitter and the receiver is varied. The error rate for the various modulation schemes are calculated as a function of this range.

Jamming Scenario

The previous section described the transmitter/receiver scenario to assess the relative performance of various modulation methods at millimeter wavelengths without jamming. This section adds jamming to determine the extent of performance degradation. One way for a jammer to disrupt a digital communication system is to increase the bit error rate to an intolerable level. According to information theory, the most destructive type of additive noise in a communication system is white Gaussian noise (Reference 23: 6). The jamming is modeled as bandlimited white Gaussian noise. This allows well-known theoretical formulas to determine the impact of jamming on millimeter wave communications. Thus, the effects on digital data transmission of a white Gaussian jammer can be analyzed in a straight forward fashion.

The Jammer/Transmitter/Receiver model is illustrated in Figure III-1. The jammer is positioned behind the transmitter on the same

line-of-sight path, aiming its signal directly into the receiving antenna's main lobe. This arrangement provides a worst case arrangement as well as simplifying the geometry.

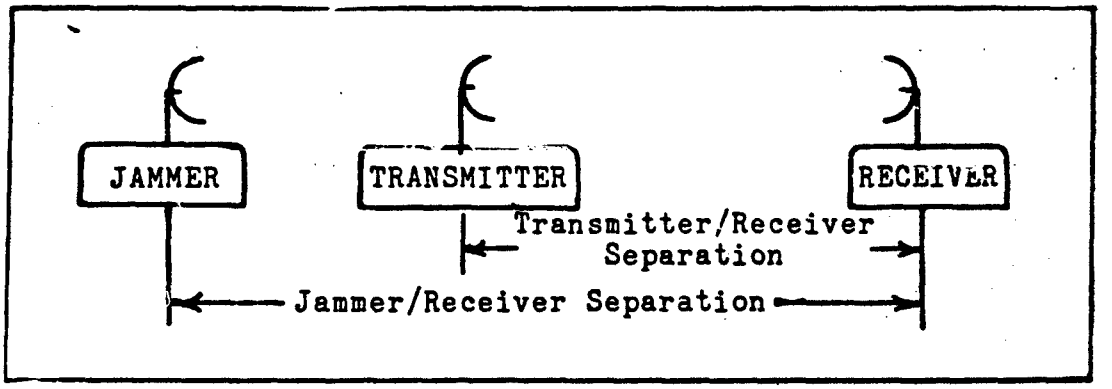

Fig. III-1. Channel Model for Jamming Environment.

Input Parameters

The program begins with a brief description of its algorithm. The user is then prompted for the input parameters. The input parameters required for execution of the algorithm are: 1) The carrier frequency in gigahertz; 2) The attenuation factor in decibels per kilometer; 3) The transmitter power level in milliwatts; 4) The transmitting antenna's gain in decibels; 5) The receiving antenna's gain in decibels; 6) The system bandwidth in Hertz; 7) The particular modulation technique to be used (1 - binary coherent ASK and FSK, 2 - binary coherent PSK, 3 - binary noncoherent ASK and FSK, 4 - DPSK, 5 - QPSK); 8) A set of range values given in the form of an initial range, final range, and a range delta; 9) The jammer's power level in milliwatts; 10) The jammer's antenna gain in decibels; 11) The distance of the jammer in kilometers from the receiver.

After all information has been entered, the program displays the input data. The user may make any corrections as required; however, all information must be re-entered. All inputs are self-explanatory. Input 8 requires the final range to exceed the initial range. The program will now calculate the bit error rate as a function of the transmitter range from the receiver. Once a calculation is made for a given range, the program stores the results, updates the range value, and repeats until the range value reaches the final range.

Calculation of the Received Power Level

The calculation of the received power level is accomplished through the use of the procedure named CALCULATERECEIVEDPOWERdBm.

Procedure CALCULATERECEIVEDPOWERdBm. When the calculation of the received power level at the receiver/antenna junction is required, the main program calls the procedure CALCULATERECEIVEDPOWERdBm. This procedure requires six passed input variables from the main program for execution. These inputs are the transmit power of the source in mW, P_t; both of the transmitting/receiving antenna gains in dB, G_t and G_r; the operating frequency in GHz, f; the attenuation factor in dB/km, α; and a range value, R. The received power level, P_r, is calculated by inter-relating these inputs using the familiar link equation:

$$P_r\ (\text{dBm}) = 10 * \log(P_t) + G_t + G_r + 10 * \log(\lambda^2/(4{,}000\pi R)^2) - \alpha R \qquad (3.1)$$

where wavelength λ (meters) = (speed of light)/f. The link equation is discussed more thoroughly in Chapter 2 (see Pages II-20 through II-25). The received power level in dBm is returned to the main program.

Calculation of the Signal-to-Noise Ratio

The calculation of the signal-to-noise ratio is accomplished through the use of the procedure named FINDSNR.

Procedure FINDSNR. This procedure is called by the main program once the received power levels in dBm are found. This procedure requires three inputs for execution. These inputs are the received signal power level from the transmitter, the received jammer power level, and the bandwidth of the system. The received signal power level is treated as the average signal power per bit. The received jammer power is considered as an independent noise power J placed in each signaling band. The noise level N is calculated from equation 2.26 repeated here:

$$N = P_{int} = -174 \text{ dBm} + 10 \log (\text{bandwidth}) \qquad (3.2)$$

where bandwidth is given in Hertz. The derivation of equation 2.3 is explained more fully in Chapter 2 (see Pages II-26 to II-28). The total power from noise is the sum (N + J). Therefore,

$$z = \frac{S}{(N + J)} \qquad (3.3)$$

where z is the received signal-to-noise ratio (SNR) per information bit.

Calculation of the Bit-Error Rate

The calculation of the bit-error rate for a particular modulation scheme is accomplished through the use of the procedure named CALCULATEBITERROR and the function named ERFC(x).

FUNCTION ERFC(x). The exact analytical expression for bit-error rates for binary coherent ASK, binary coherent FSK, binary coherent PSK, and QPSK may all be expressed in terms of the complementary error function. When the calculation of the complementary error function is required, the function ERFC(x) is called by the procedure CALCULATEBITERROR. The function requires a non-negative real number argument for proper execution. The procedure CALCULATEBITERROR provides error protection to insure that it uses only non-negative arguments when calling ERFC(x). The function itself contains some minor error checking. If a negative number is encountered, the function will return an error message to warn the user of the bad data point resulting from the attempt to send a negative argument to ERFC(x). Due to the importance of this particular function, a detailed discussion of the Pascal-coded algorithm may be found in Appendix A of this thesis.

Procedure CALCULATEBITERROR. This procedure calculates the probability of a bit-error for five modulation schemes. The schemes available are: 1 - binary coherent ASK and FSK, 2 - binary coherent PSK, 3 - binary noncoherent ASK and FSK, 4 - DPSK, and 5 - QPSK. The main program calls this module with two input variables. These required inputs are the flag number associated with the particular bit-error rate and the average signal-to-noise ratio calculated through procedure FINDSNR. Since input SNR is in terms of decibels, this value must be converted to the received power ratio z by the relationship

$$SNR = 10 * \log z \qquad (3.3)$$

when rearranged becomes

$$z = 10^{(SNR/10)} \tag{3.4}$$

resulting in a positive number. This simple operation provides the necessary error-protection for the function ERFC(x) which requires a non-negative argument.

The method used to calculate the error-rate depends on the type of digital signaling. Two well-known types of binary digital signaling are commonly used. These are called "antipodal" and "orthogonal".

The performance of antipodal binary signals on the AWGN channel is

$$P_b = \frac{1}{2}\,\text{erfc}\sqrt{\frac{\alpha^2 \epsilon_b}{N_0}} = \frac{1}{2}\,\text{erfc}\,(\sqrt{z}) \tag{3.5}$$

where $z = \alpha^2 \epsilon_b / N_0$ is the received signal-to-noise ratio (SNR) per information bit. Antipodal signals are usually generated via binary coherent phase-shift keying (PSK). PSK is achieved by shifting the phase of the carrier through some arbitrary angle to represent a "1" and the same angle plus 180 degrees to represent "0". The signal waveforms can be written as

$$\begin{aligned} S1 &= A \sin(2\pi f_L t + \theta) \qquad 0 \le t \le T \\ S2 &= A \sin(2\pi f_L t + \theta + \pi) \qquad 0 \le t \le T \end{aligned} \tag{3.6}$$

Figure III-2 illustrates a PSK signal with $\theta = 0$. Orthogonal signaling has probability of error for phase-coherent detection of

$$P_b = \frac{1}{2}\,\text{erfc}\,(\sqrt{z/2}) \tag{3.7}$$

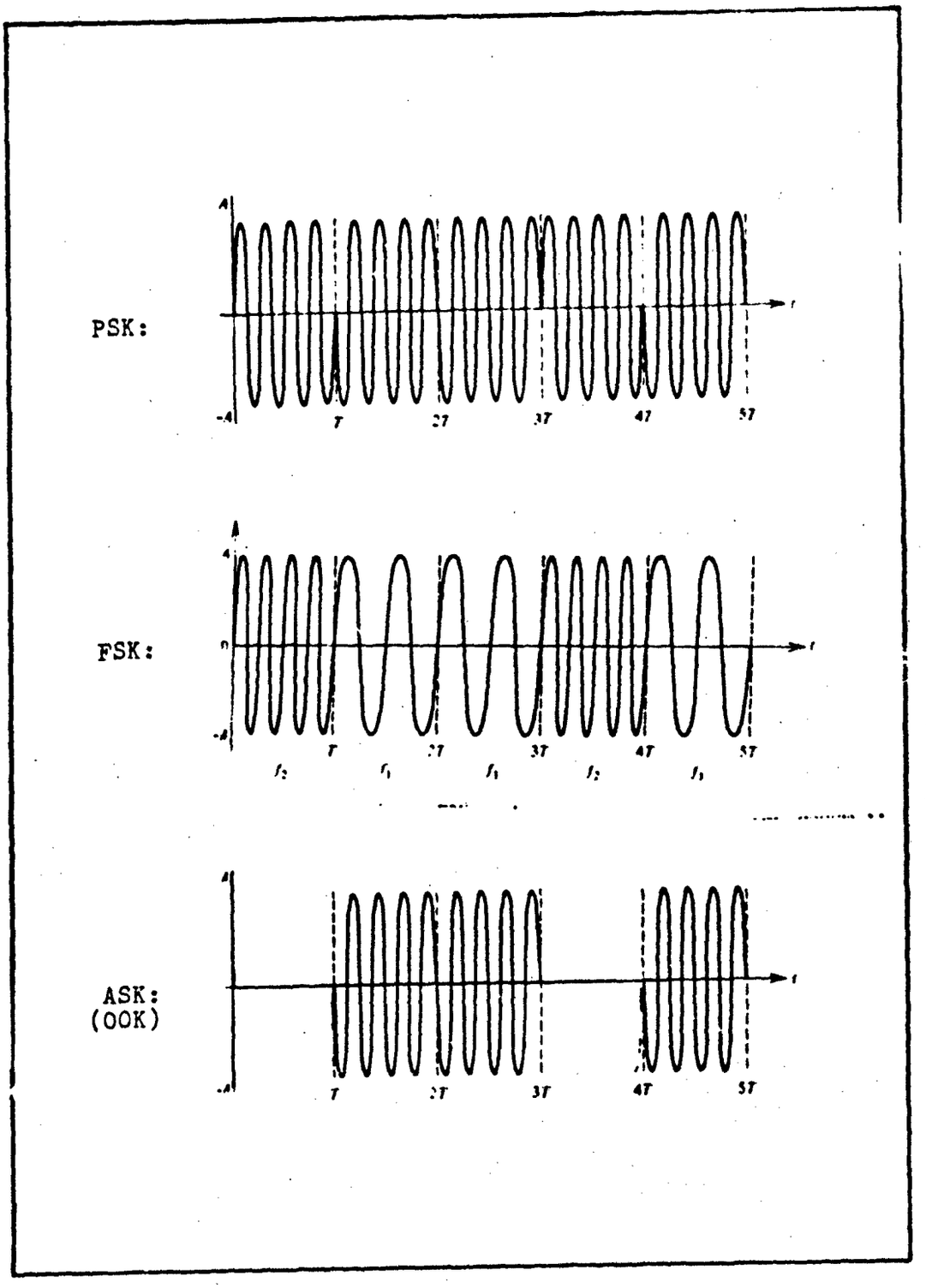

Fig III-2. Example of binary PSK, FSK, and ASK (OOK).

Orthogonal signaling is 3 dB poorer than the performance of antipodal signaling due to the factor 1/2 under the radical in the argument of the error function. This is shown in Figure III-3. A common modulation technique of the orthogonal type is binary coherent frequency-shift keying (FSK). In FSK, the binary information is represented by two different frequencies. The waveforms can be represented as

$$\begin{aligned} S1 &= A \sin(2\pi f_1 t) \qquad 0 \le t \le T \\ S2 &= A \sin(2\pi f_2 t) \qquad 0 \le t \le T \end{aligned} \tag{3.8}$$

where $f_1 = f_L - \Delta f/2$, $f_2 = f_L - \Delta f/2$. The minimum frequency separation for orthogonality with coherent detection is $\Delta f = (1/2T)$ Hz. Figure III-2 also illustrates a FSK signal. Another modulation technique of the orthogonal type is binary coherent amplitude-shift keying (ASK) in the form of the on/off keying (OOK). In OOK, two amplitudes are used to represent the binary information, one of these being zero. In general, the signals for ASK are

$$\begin{aligned} S1 &= A1 \sin(2\pi f_L t) \qquad 0 \le t \le T \\ S2 &= A2 \sin(2\pi f_L t) \qquad 0 \le t \le T \end{aligned} \tag{3.9}$$

In Figure III-2, S1 and S2 for OOK are shown with A1 = 0 and A2 = A. Henceforth, binary ASK refers to an OOK implementation.

There are several binary modulation schemes which do not require coherent references. Two such types are known as non-coherent ASK and FSK. Also, the scheme differentially coherent phase-shift keying (DPSK) may be thought of as the non-coherent version of PSK. A truly non-conerent PSK system does not exist since it would be impossible to send information in the phase of a carrier of completely random phase.

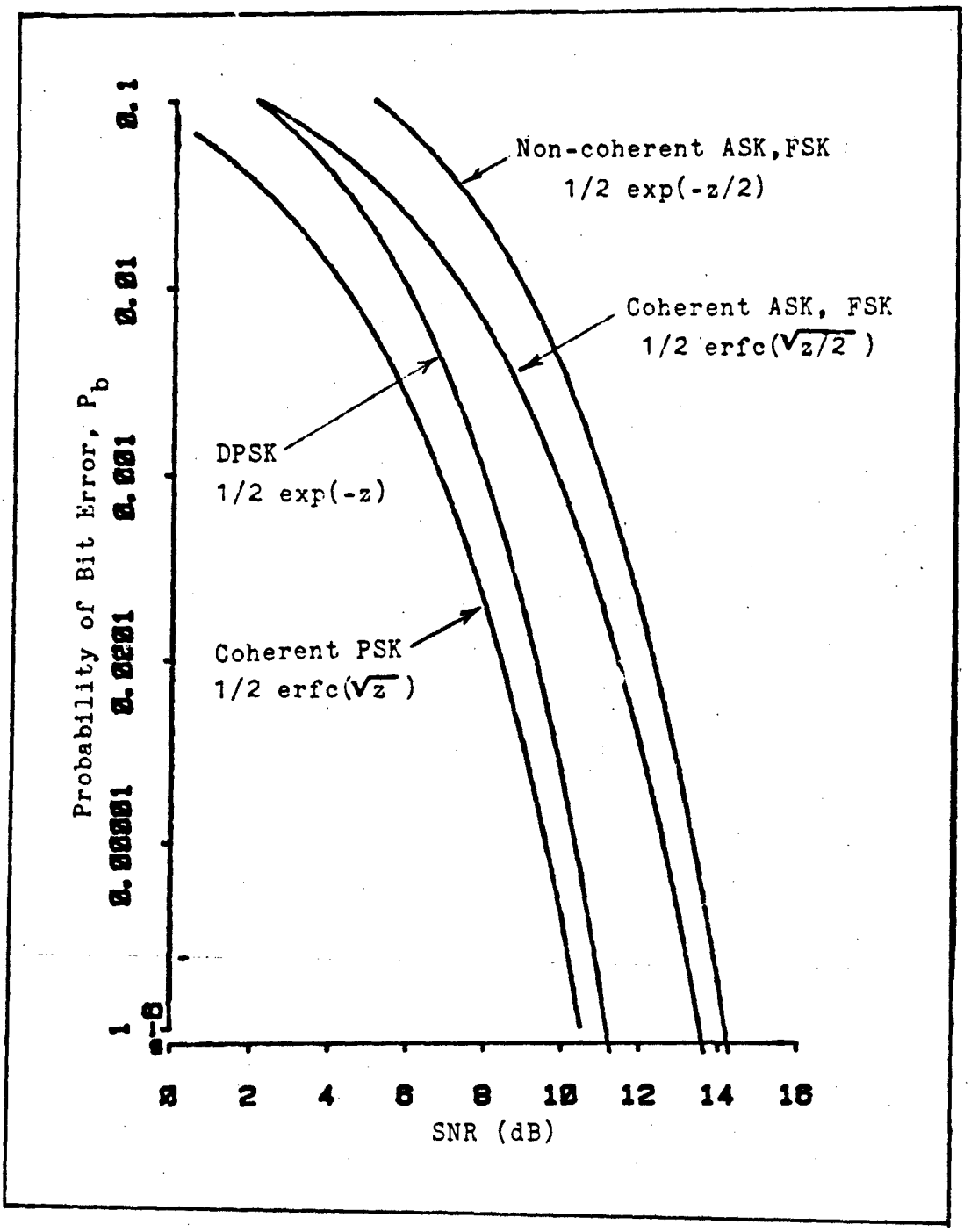

Fig III-3. Error probabilities for several binary signaling schemes.

For non-coherent ASK and FSK, the probability of error is

$$P_b = 1/2 \exp(-z/2) \tag{3.10}$$

It is interesting to compare this result with the asymptotic expansion of the complementary error function. For coherent ASK and FSK, the approximation for large SNRs using the asymptotic expansion is

$$P_b = \sqrt{\frac{2}{\pi z}}\ 1/2 \exp(-z/2), \quad z \gg 1 \tag{3.11}$$

This indicates that non-coherent ASK and FSK suffers a loss of less than 1 dB over coherent ASK and FSK at high SNRs as shown in Figure III-3.

For DPSK, phase reference is obtained by using the carrier phase of the previous signaling interval. The result for the error probability is

$$P_b = 1/2 \exp(-z) \tag{3.12}$$

Recalling the coherent PSK error probability using the asymptotic expansion for erfc(x), the following result is obtained:

$$P = \frac{1}{(\sqrt{\pi z})}\ 1/2 \exp(-z), \quad z \gg 1 \tag{3.13}$$

Thus for large SNRs, DPSK and coherent PSK differ only by the factor $1/\sqrt{2}$, indicating a loss of less than 1 dB as shown in Figure III-3.

Binary digital communication systems can transmit one of only two possible signals during each signaling interval. In an M-ary system, one of M possible signals may be transmitted where $M > 2$. One of the most common M-ary systems is four-phase PSK or quadrature PSK (QPSK).

QPSK can be viewed as two binary PSK systems with carriers in phase quadrature. Thus, the probability of bit error is identical to equation 3.5. That is,

$$P_b = 1/2 \text{ erfc}(\sqrt{z}) \tag{3.14}$$

The symbol error probability for QPSK is determined by noting that

$$\begin{aligned} P_c &= (1 - P_b)\ (1 - P_b) \\ &= [1 - 1/2 \text{ erfc}(\sqrt{z})]^2 \end{aligned} \tag{3.15}$$

Where P_c is the probability of correct reception. This result has assumed that the errors in the quadrature channels are independent. Therefore, the symbol error probability for QPSK is

$$\begin{aligned} P_4 &= 1 - P_C \\ &= \text{erfc}(\sqrt{z})[1 - 1/4 \text{ erfc}(\sqrt{z})] \end{aligned} \tag{3.16}$$

Chapter 4: Results

Introduction

This chapter compares the transmission performance of millimeter waves using the digital signaling techniques presented in Chapter 3. This comparison is based on the maximum separation between the transmitter and receiver in kilometers required to achieve a specified probability-of-error. For this comparison to be meaningful, the system parameters with the exception of the transmitter/receiver separation are kept fixed. And when applicable, the jammer's distance from the receiver is also variable. This chapter begins with a description of the system parameters chosen for this study. Next, performance comparisons are made for the transmitter/receiver link without jamming interference. Finally, the performance comparisons are repeated in the presence of a jammer as discussed in the jamming scenario of Chapter 3.

System Parameters

From the discussion in Chapter 2, a communication link strongly depends upon the particular system's parameters. Namely, the transmitter's output power level, the system's bandwidth, and the transmitting and receiving antenna's gain. For this investigation, these parameters were chosen to reflect a low-power system transmitting low data-rates. Unless otherwise indicated, all results were obtained with the same set of system parameters. These are:

Transmit power = 100 milliwatts

Transmitting antenna gain = 30 decibels

Receiving antenna gain = 30 decibels

Bandwidth = 100 Hertz

Transmitter/receiver separation = (variable) kilometers

Jammer/receiver separation = (variable) kilometers

Jammer power level = (variable) milliwatts

Jamming antenna gain = 30 decibels

Performance Comparisons of Millimeter Wave Data Link

In this section, the performance of the transmitter/receiver link operating at millimeter wavelengths is illustrated. Figures IV-1 through IV-4 show the bit error curves as a function of the transmitter/receiver separation for several frequency/altitude combinations. Values for these inputs were obtained from Table II-2 of this thesis which lists the attenuation rates at the oxygen resonant frequencies. The curves in each figure represent the different binary signaling schemes addressed in study. These curves can be grouped into a set of four curves. Each group of four curves is the output for a particular frequency/altitude combination or, equivalently, a frequency/attenuation-rate combination since the attenuation rate is a function of altitude. Recall the attenuation rate decreases with an increase in altitude allowing greater separation between the transmitter and receiver. Figure IV-1 presents a set of performance curves for a frequency of 60.4343 GHz at sea level (altitude = 0 km, attenuation rate = 16.1843 dB/km). For convenience since this set of curves remain fixed in relation to each other, each curve is labeled with its respective signaling method in this figure only. It should be pointed out that Figure IV-1 is quite similar to the typical error-probability versus signal-to-noise ratio curve such as shown in Figure III-3 of this thesis. In fact, these curves can easily be shown to be identical. To

see this, the transmitter/receiver seperation axis must be translated into their equivalent signal-to-noise ratios. This relationship is shown in Table IV-1 below:

Table IV-1. Relationship between the tranmsitter/ receiver separation and the signal-to-noise ratios.

Transmitter/receiver separation	Signal-to-noise ratio
4.80	14.622
4.90	12.824
5.00	11.030
5.10	9.240
5.20	7.542
5.30	5.669
5.40	3.888
5.50	2.110
5.60	0.335
5.70	-1.437
5.80	-3.207
5.90	-4.974
6.00	-6.738
6.10	-8.500
6.20	-10.260
6.30	-12.017
6.40	-13.773
6.50	-15.526

For the coherent PSK and DPSK curves in Figure IV-1, a sharp increase in the bit-error rate is seen when the transmitter/receiver separation increases beyond 5.15 km. The same effect occurs for the coherent and non-coherent versions of the ASK and FSK signaling schemes around 5 km. Since these values are for a clear, non-turbulent atmosphere, this establishes a limit on the communication range between transceivers. Shown in Figure IV-2 are the curves for the system addressed in Figure IV-1. The curves are redrawn and compared with an identical system with receiver gains of 75 dB and 150 dB, an increase of

45 dB and 120 dB respectively. This demonstrates the large change required to obtain a small increase in the transmitter/receiver separation for frequencies near the peak of the oxygen absorbtion band. It is interesting to note that to obtain equivalent performance with an increase in the transmitted power level would require 31.623 kilowatts to match the 2.25 km increase in separation and one million megawatts to increase the separation to 12 km. Thus, since little radiation seems to reach beyond the separation limit, such a communication link could operate with little interference from other systems operating at the same frequency provided that the communication zones do not overlap. In Table IV-2, the frequencies of Table II-2 are listed with their limits on the communication range in a clear non-turbulent atmosphere for various altitudes. These limits were established by locating the transmitter/receiver separation that gives a probability-of-error of 10^{-4} for coherent PSK.

Figure IV-3 illustrates three of the limits presented in Table IV-2. The three sets of performance curves are for frequencies of 54.1294 GHz, 53.0695 GHz, and 52.0259 GHz (attenuation rate = 2.2495 dB/km, 1.1218 dB/km, and 0.6096 dB/km respectively).

Figure IV-4 presents four sets of performance curves for a frequency of 60.4348 GHz at altitudes of 8 km, 12 km, 16 km, and 20 km (attenuation rate = 13.5369 dB/km, 10.8101 dB/km, 7.4704 dB/km, and 5.3018 dB/km respectively). This shows the increase communication range of millimeter waves by operating at a higher altitude.

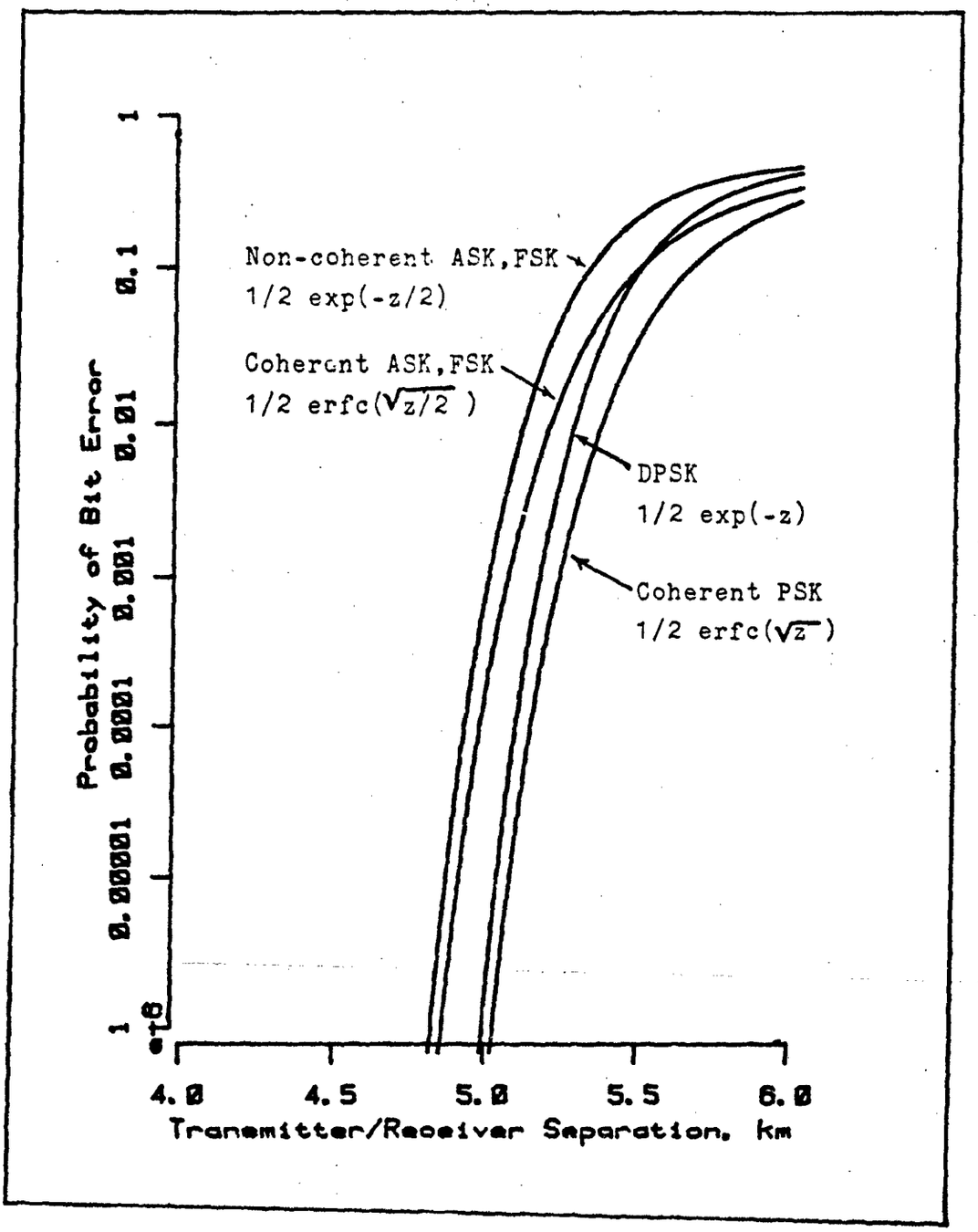

Figure IV-1. Frequency = 60.4348 GHz. Attenuation = 16.1843 dB/km. Performance curves for several signaling schemes.

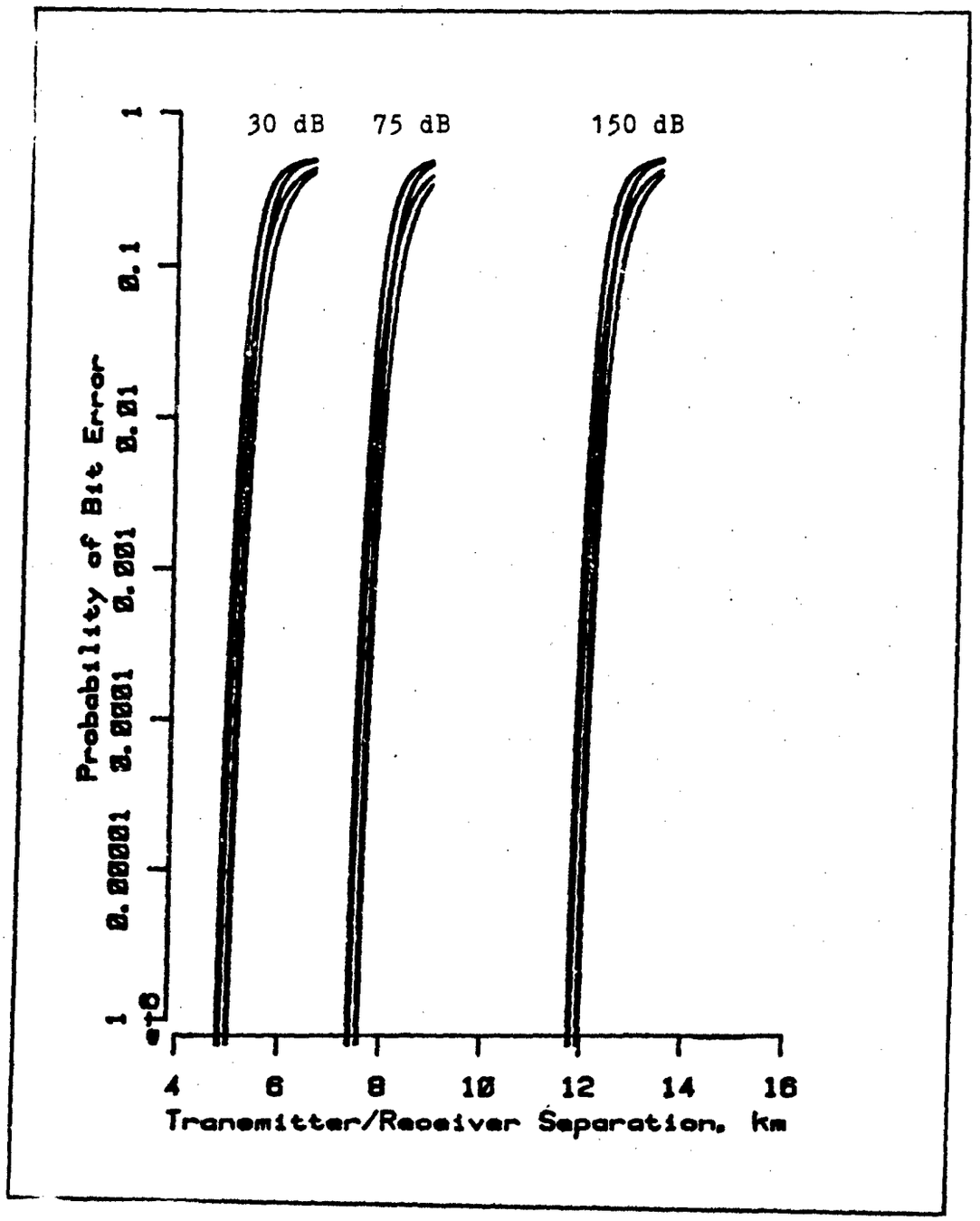

Figure IV-2. Comparison between systems with additional receiving antenna gains.

Table IV-2. Maximum horizontal transmitter/receiver separation in km at oxygen resonant frequencies.

FREQ. (GHz)	Altitude, km 0	4	8	12	16	20
48.4530	297.067	552.136	1077.845	1964.294	4854.756	23825.456
48.9582	264.377	493.473	969.098	1772.715	4202.181	21315.746
49.4648	233.235	437.784	825.415	1593.887	3716.257	15479.117
49.9730	203.373	383.985	763.419	1413.303	3309.267	11318.449
50.4830	174.768	332.403	666.912	1244.137	2920.410	9686.750
50.9949	147.357	282.164	571.881	1080.022	2519.074	7628.715
51.5091	121.240	233.228	478.171	914.646	2128.895	5777.453
52.0259	96.956	186.190	384.486	745.669	1695.520	3911.430
52.5458	75.197	142.559	293.357	575.312	1244.831	2551.195
53.0695	56.689	104.551	210.261	411.190	826.247	1456.629
53.5960	41.880	74.073	142.494	272.385	500.921	785.269
54.1294	30.577	51.322	92.773	169.933	287.704	414.553
54.6728	22.258	35.219	59.248	102.753	163.159	223.220
55.2214	16.336	24.319	37.997	62.140	94.436	125.225
55.7839	12.036	16.575	23.825	36.742	55.271	73.131
56.2648	9.681	12.180	15.040	20.333	29.156	41.181
56.3634	9.395	11.804	14.547	19.700	27.778	37.757
56.9682	8.263	10.636	13.676	18.987	26.257	32.803
57.6125	7.176	8.976	11.007	14.626	19.836	24.493
58.3239	5.996	6.788	7.330	9.062	12.485	16.684
58.4466	5.925	6.748	7.395	9.255	13.259	18.775
59.1642	5.732	6.808	7.934	10.156	14.078	17.687
59.5910	5.598	6.719	7.963	10.251	14.457	18.366
60.3061	5.156	5.727	6.096	7.491	10.563	14.589
60.4348	5.147	5.707	6.050	7.413	10.340	14.065
61.1506	5.691	7.009	8.398	10.877	14.735	18.186
61.8002	5.839	8.398	9.088	12.247	16.966	21.228
61.4112	5.796	6.733	7.521	9.529	12.964	17.571
62.4863	5.857	6.779	7.540	9.445	12.654	16.627
62.9980	7.078	9.274	12.691	18.829	28.829	37.320
63.5685	9.271	13.143	19.320	30.016	44.505	58.061
64.1272	12.084	18.125	28.486	46.745	71.242	94.632
64.6779	15.907	25.286	42.715	74.271	118.633	162.965
65.2240	21.137	35.592	64.529	118.432	202.007	292.899
65.7626	28.043	49.723	95.841	183.391	339.993	535.793
66.2978	36.815	68.015	136.949	268.036	561.137	962.620
66.8313	47.346	89.845	184.937	362.855	792.607	1597.599
67.3627	59.193	113.744	235.033	456.409	1048.663	2459.401
67.8923	71.786	138.189	283.574	543.178	543.178	1274.655
68.4205	84.632	162.228	329.314	623.116	1476.428	4318.211
68.9478	97.414	185.532	372.803	699.095	1657.938	5425.279
69.4741	110.001	208.150	415.111	772.791	1828.367	6630.751
70.0000	122.419	230.317	456.285	845.617	2012.282	8442.287
70.5249	134.719	252.259	497.205	916.812	2217.783	10508.307
71.0497	146.917	273.996	537.780	987.428	2445.075	13513.417

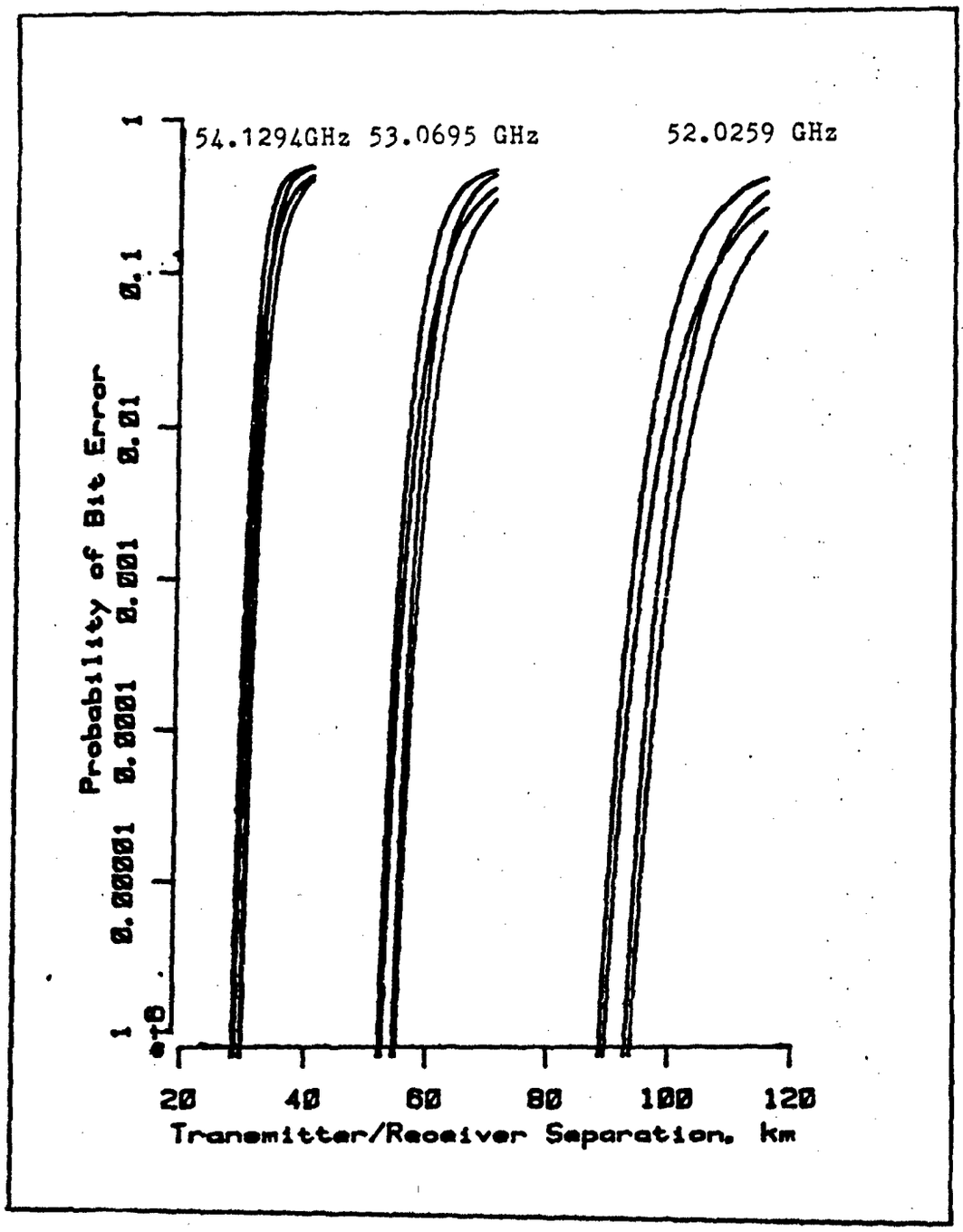

Figure IV-3. Performance curves for frequencies of 54.1294, 53.0695, and 52.0259 GHz at sea level.

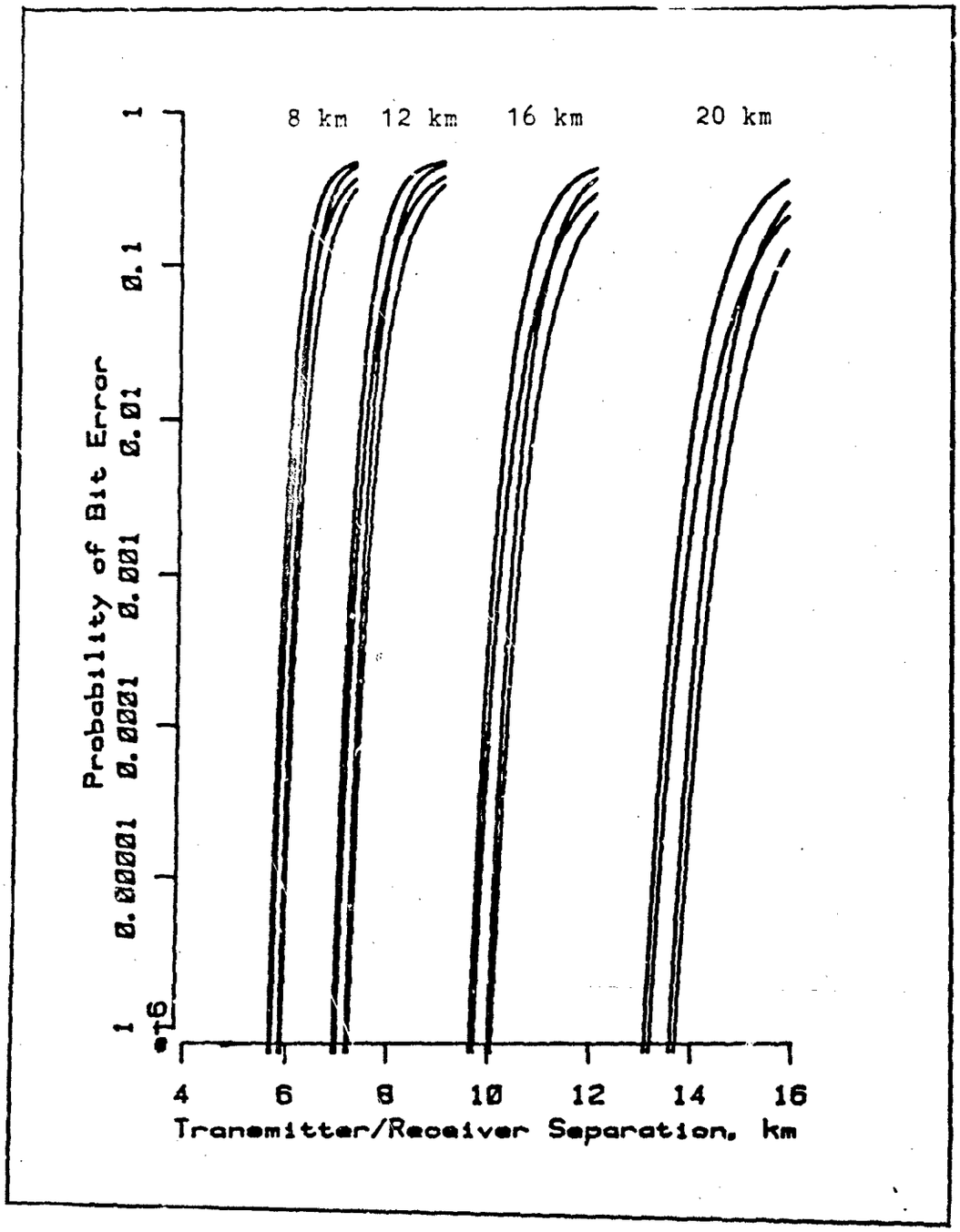

Figure IV-4. Performance of 60.4348 GHz at altitudes of 8, 12, 16, and 20 km.

Performance Comparisons With Jamming

In this section, the performance of millimeter waves in the presence of a jammer is shown. Figure IV-5 shows the high power a jammer must possess in order to reduce the transmitter/receiver separation to less than 0.5 km for a frequency of 60.4348 at sea level. Two sets of curves are presented. One case with 100 watt jamming and the other with 10 million watt jamming. The jammer was given a close range located 10 km from the receiver. The 100 watt jammed signal when compared with Figure IV-1, the unjammed case, shows little or no reduction in the separation. The large powered jammer shows only a small decrease of approximately 0.5 km.

Figure IV-6 presents a frequency of 53.0695 at sea level. The two sets of curves are as before. One with a 100 watt jammer and the other with a 10 million watt jammer. The jammer for this case was located at 100 km from the receiver. Frequencies with relatively small attenuation are seen to be more strongly affected by the high powered jammer; yet, modest powered jammers have little effect on reducing the transmitter/receiver separation.

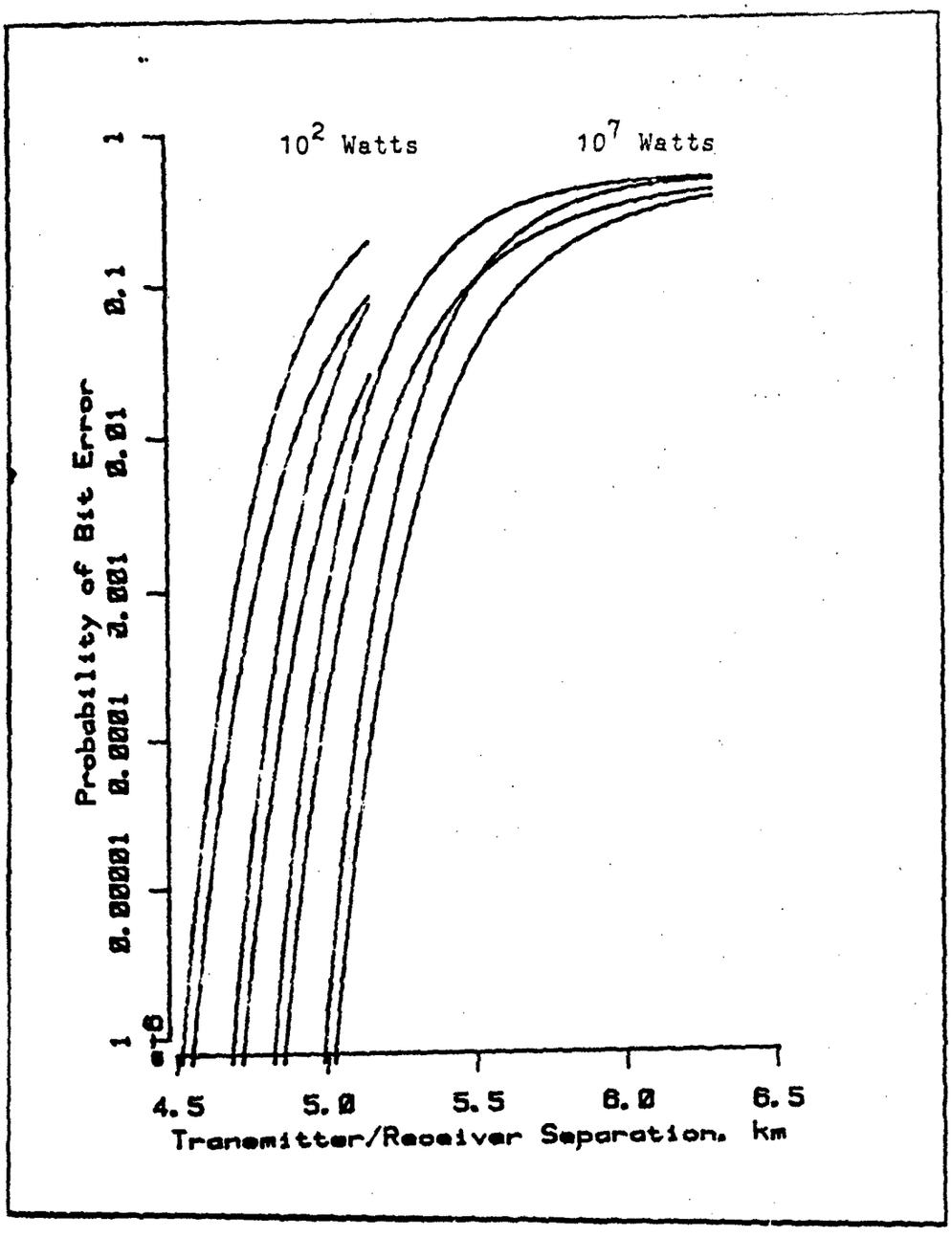

Figure IV-5. Performance of 60.4348 GHz in the presence of jamming. Jammer located at 10 km.

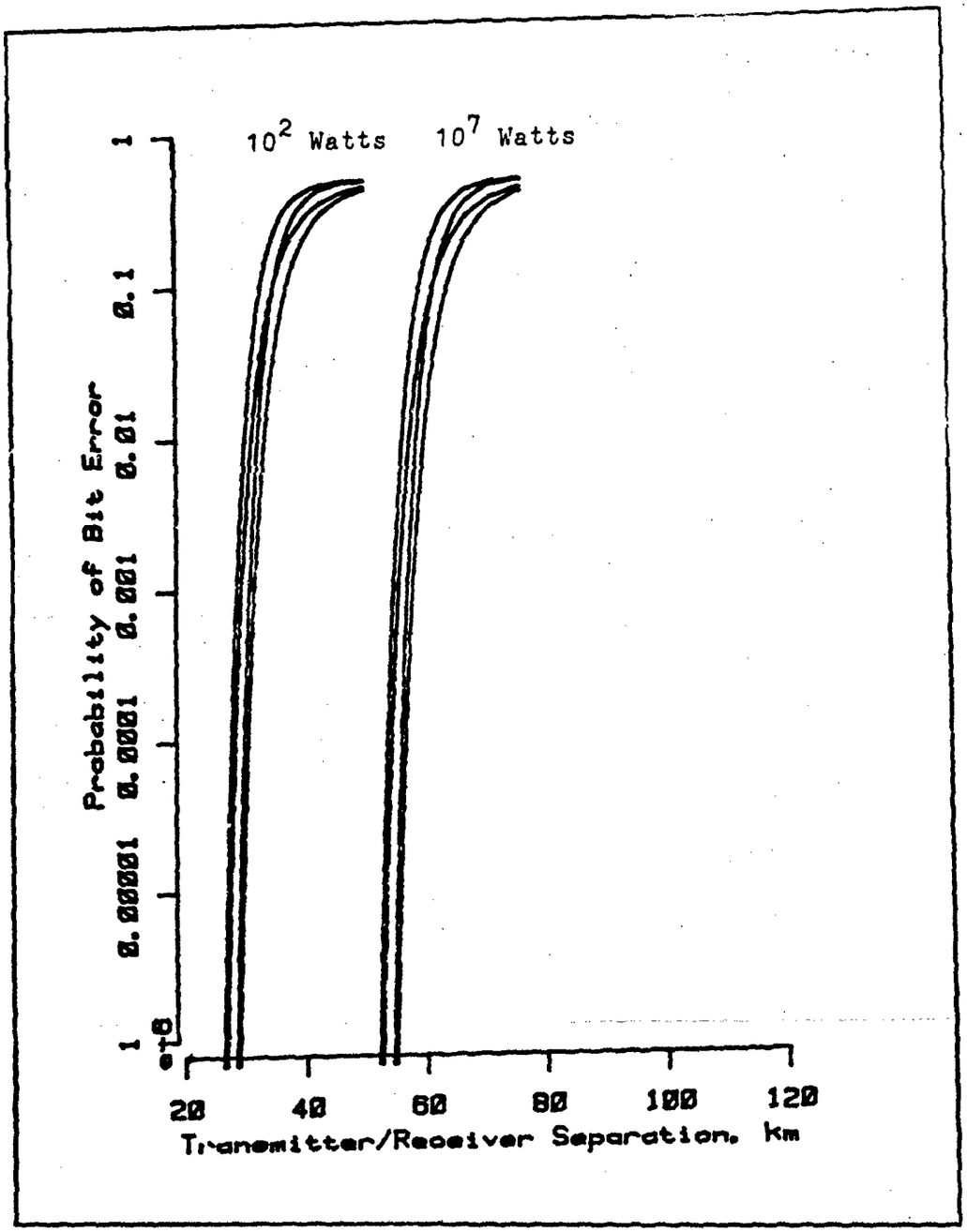

Figure IV-6. Performance of 53.0695 GHz in the presence of jamming. Jammer located at 100 km.

Chapter 5: Conclusions

Conclusions

The objective of this thesis was to determine the maximum communication link, i.e., transmitter/receiver separation in a non-turbulent, clear atmosphere for a given probability of error for various binary signaling techniques for a low-power, low data-rate system and then compare the results to those obtained in the presence of a jammer. The communication link was calculated by developing a general algorithm following the familiar link equation and accounting for the atmospheric attenuation property of millimeter waves. Results were obtained for a variety of cases around the 60 GHz oxygen resonant absorbtion band for several altitudes to 20 kilometers in the form of tables and plots of probability-of-error versus the transmitter/receiver separation.

It has been demonstrated that two solutions to increase the communication range of a particular millimeter wave system are available assuming a fixed frequency. One, upgrade some combination of system parameters such as an increase in the transmitter's output power level. This might prove to be too costly in terms of money or space depending on the frequency range. This study has shown that for systems operating at frequencies near the 60 GHz attenuation peak require tremendous output power increases to obtain marginal increases in transmitter/receiver separation. The other alternative is moving communications to a higher altitude to take advantage of the reduced attenuation. However, for most cases, this could easily be unfeasible.

Although for aircraft-to-aircraft data transfer applications, the simpler solution might be to operate at a higher altitude. Of course, this would depend on the frequency being used. Figure IV-3 illustrated that two aircraft operating at a frequency near the peak of the 60 GHz absorbtion band would have to fly above 16 km to double the maximum range they had at sea level. A much easier solution is to have a system with a tunable frequency. This would provide much better control on ranging a communication link than changing altitude. For many channels, a 3 dB increase in received signal-to-noise ratios is often sought. In the millimeter wave channel, it has been shown that a 3 dB increase gain is inconsequential in terms of transmitter/receiver separation. Thus, because of the comparable performance and added simplicity of non-coherent modulation methods, these techniques should be used over the more costly and complex coherent systems. For the same reason, the application of spread spectrum techniques or coding techniques as a means to improve the performance of millimeter waves is not needed.

On the basis of this study, it is concluded that jamming has a limited effect on millimeter wave communications depending upon the frequency. These frequencies provide high jam and interference protection because of their narrow beamwidths and the high oxygen absorbtion losses encountered by jammers. To be more effective for frequencies near the oxygen absorbtion peak, a jammer requires enormous amounts of power and be positioned very close to the target receiver. Due to the small beamwidths and corresponding small sidelobes of millimeter waves, a jammer must be located "uncomfortably" close to intercept a sidelobe.

References

1. Epsztein, B., et al. "Round Table Discussion on Future Trends and Applications of Millimeter Wave Research," Proceedings of the Symposium on Millimeter Waves, Volume IX, Microwave Research Institute Symposia Series. Edited by Jerome Fox and Martha Crowell. 650-651. Brooklyn: Polytechnic Press, 1960.

2. Chase, Michael R. and Schneider, Mark J. Terrestrial Millimeter-Wave Communication Systems for the Navy. MS Thesis. Monterey, California: Naval Postgraduate School, June 1980 (AD 8047 464).

3. Kuno, H.J., "IMPATT Devices for Generation of Millimeter Waves," Infrared and Millimeter Waves: Volume 1, Sources of Radiation. Edited by Kenneth J. Button. New York Cotey: Academic Press, 1979.

4. Wiltse, James C. "Introduction and Overview of Millimeter Waves," Infrared and Millimeter Waves, Volume 1, Millimeter Systems. New York City: Academic Press, 1981.

5. Altshuler, Edward E., et al., "Atmospheric Effects on Propagation at Millimeter Wavelengths," IEEE Spectrum: 83-90 (July 1968).

6. Bostian, C.W., et al., The Influence of Polarization on Millimeter Wave Propagation Through Rain: NASA Grant Number NGR-47-004-091. Blacksburg, Virginia: Electrical Engineering Department, Virginia Polytechnic Institute and State University, January 1974.

7. Fedi, Francesco, "Prediction of Attenuation Due to Rainfall on Terrestial Links," Radio Science: Volume 16, Number 5, 731-743 (September-October 1991).

8. Stutzman, W.L. and Dishman, W.K., "A Simple Model for the Estimation of Rain-Induced Attenuation Along Earth-Space Paths at Millimeter Wavelengths," Radio Science: Volume 17, Number 6. 1465-1476. (November-December 1982).

9. Olsen, Roderic L., et al., "The aR^b Relation in the Calculation of Rain Attenuation," IEEE Transactions on Antennas and Propagation: Volume AP-26, Number 2, 318-329 (March 1978).

10. Crane, Robert K., "The Rain Range Experiment -- Propagation Through a Simulated Rain Environment," IEEE Transactions on Antennas and Propagation: Volume AP-22, Number 2, 321-328 (March 1974).

11. Crane, Robert K., "A Two-Component Rain Model for the Prediction of Attenuation Statistics," Radio Science: Volume 17, Number 6, 1371-1387 (November-December 1982).

12. EHF Air-to-Air Communications Techniques: Final Technical Report: Volume I (of three). Hughes Aircraft Company RADC-TR-82-314. (November 1982).

13. Reber, E.E., Mitchell, R.L., and Carter, C.J., "Oxygen Absorption in the Earth's Atmosphere," Microwave Journal: 73-81 (November 1968).

14. Crane, Robert K., "Fundamental Limitations Caused by RF Propagation," Proceedings of the IEEE: Volume 69, Number 2, 196-209 (February 1981).

15. Measured Effects of Battlefield Dust and Smoke on Visible, Infrared, and Millimeter Wavelength Propagation: A Preliminary Report on Dusty Infrared Test - I: Compiled by James D. Lindberg (AD-B035 420L) (January 1979).

16. Near-Millimeter Wave Technology Base Study: Volume I - Propagation and Target Background Characteristics: Kulpa, Stanley M., and Brown, Edward A. (AD-A079 620) (November 1979).

17. Thomson, James H., "Dust Clouds - Models and Propagation Effects," Proceedings of the Workshop on Millimeter and Submillimeter Atmospheric Propagation Applicable to Radar and Missile Systems, Held at Redstone Arsonal, Alabama, 20-22 March 1979: Essenwanger, Oskar M. Essenwanger and Stewart, Dorothy A. (Editors). U.S. Army Missile Laboratory technical report RR-80-3 (AD-A087 754), 100-108 (February 1980).

18. Gallaghev, J.J., McMillan, R.W., Rogers, R.C., and Snider, D.E., "Measurements of Attenuation Due to Simulated Battlefield Dust at 94 and 140 GHz," Proceedings of the Workshop on Millimeter and Submillimeter Atmospheric Propagation Applicable to Radar and Missile Systems, Held at Redstone Arsonal, Alabama, 20-22 March 1979: Essenwanger, Oskar M. Essenwanger and Stewart, Dorothy A. (Editors). U.S. Army Missile Laboratory technical report RR-80-3 (AD-A087 754), 114-117 (February 1980).

19. Lin, Sing H., "Empirical Rain Attenuation Model for Earth-Satellite Paths," IEEE Transactions on Communications: Volume COM-27, Number 5, 812-817 (May 1979).

20. Ziemer, R.E. and Tranter, W.H., Principles of Communications. Boston: Houghton Mifflin Company, 1976.

21. Friis, Harold T., "30 Years With Microwaves," The Microwave Journal: Volume II, 28-32 (August 1968).

22. Miller, Alan R., Pascal Programs for Scientists and Engineers: SYBEX 1981.

23. Torrieri, Don J., Principal of Military Communications. Dedham, MA: Artec House, Inc., 1981.

Appendix A
Pascal Program: Complementary Gaussian Error Function

This appendix discusses the Pascal-coded program generated to evaluate the Gaussian error function and its complement. This program was written to operate on AFIT's VAX/11 computer system which supports the Berkley Pascal language, version 2.0. This system also hosts the IMSL Library, an extensive collection of mathematical and statistical subroutines. Both the Gaussian error function and the complementary error function are readily available from the IMSL Library; however, this library is Fortran based. Although I was unable to use the IMSL Library directly, IMSL provides an excellent means of checking the results obtained with my Pascal program. The discussion begins by reviewing the concept of the Gaussian probability distribution function.

Gaussian Probability Distribution Function

The Gaussian probability distribution function (pdf) is very useful for many engineering applications. Many naturally occuring random phenomena are Gaussianly distributed and so the Gaussian pdf is encountered frequently. Even in situations where the statistics are not Gaussian, the central limit theorem, which states that the sum of many independent random variables approaches a Gaussian-distributed variable, allows a Gaussian approximation. The Gaussian pdf is usually expressed in the form

$$p(x) = \frac{1}{\sqrt{2\pi\sigma^2}} \exp\left[-(x-m)^2/2\sigma^2\right], \quad -\infty < x < \infty \qquad (A.1)$$

where m is the mean and σ^2 is the variance of the random variable. A

plot of this function shown in Figure A-1 presents a bell-shaped curve with the area underneath equal to unity. The peak occurs at the mean value. One is often interested in the probability that x lies in the interval between (m - a) and (m + a) where a is some small positive

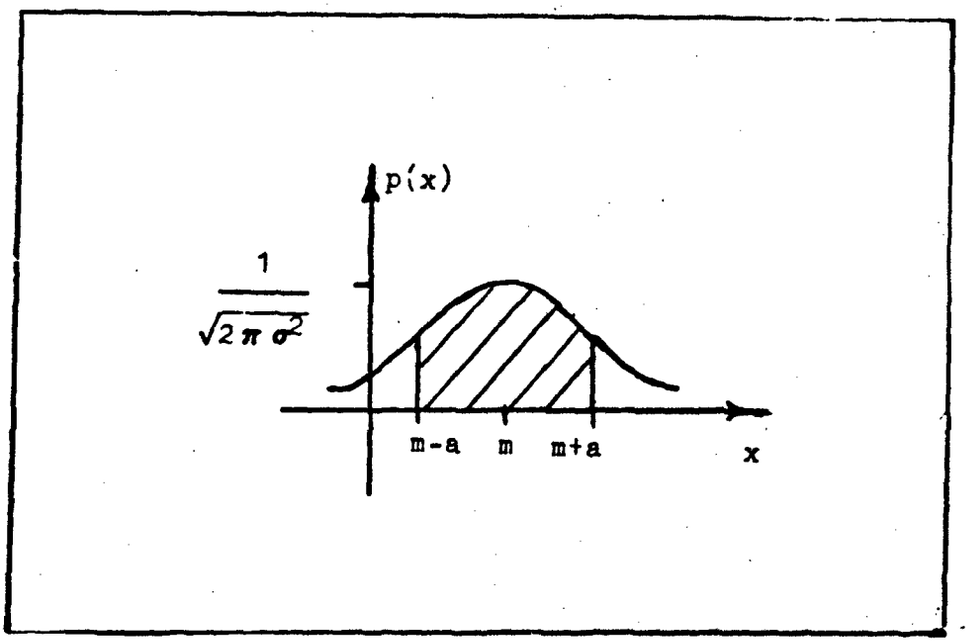

Fig. A-1. The PDF of a Gaussian-distributed random variable.

number. From equation A.1, this is written

$$P(x) = \int_{m-a}^{m+a} \frac{1}{\sqrt{2\pi\sigma^2}} \exp[-(x-m)^2/(2\sigma^2)]\, dx \qquad (A.2)$$

With the change of variables $t = (x-m)/(\sqrt{2\sigma^2})$, this integral becomes

$$P(x) = \frac{2}{\sqrt{\pi}} \int_0^y \exp(-t^2)\, dt \qquad (A.3)$$

where $y = a/(\sqrt{2\sigma^2})$. The integral in equation A.3 is called the Gaussian error function. Unfortunately, this integral cannot be

evaluated in closed form. However, it is possible to obtain particular solutions.

The Gaussian Error Function

The error function,

$$\mathrm{erf}(x) = \frac{2}{\sqrt{\pi}} \int_0^x \exp(-t^2)\, dt \qquad (A.4)$$

can be found tabulated in most mathematical handbooks. I considered evaluating the error function by substituting the series expansion for the exponential argument. The first eleven terms of such an expansion is given below:

$$\mathrm{erf}(x) = \frac{2}{\sqrt{\pi}} \left(x - \frac{1}{3}x^3 + \frac{1}{5\cdot 2!}x^5 - \frac{1}{7\cdot 3!}x^7 + \frac{1}{9\cdot 4!}x^9 - \frac{1}{11\cdot 5!}x^{11} + \frac{1}{13\cdot 6!}x^{13} - \frac{1}{15\cdot 7!}x^{15} + \frac{1}{17\cdot 8!}x^{17} - \frac{1}{19\cdot 9!}x^{19} + \frac{1}{21\cdot 10!}x^{21}\right) \qquad (A.5)$$

The accuracy varies with the argument used. The results are accurate to ten significant digits for small arguments and loses significant digits as the argument is increased. For values in the range $0.035 \le x \le 0.86$, this expansion provides results accurate to ten significant digits. Above values of 0.86, erf(x) loses significant figures quickly due to round-off errors. At the value of 1.39, the results are accurate to

only five significant digits. This creates an upper limit on the useful range of arguments. Berkley Pascal presents its own limitations as well. Real numbers can be as small as 10 to the negative 38th power and as large as 10 to the 38th power. With arguments below 0.035, the last terms of the series expansion in equation A.5 become too small for the system, thereby creating underflow errors. Thus, the useful range of arguments for this approximation is from 0.035 to 1.39.

The Complementary Error Function

The complementary error function,

$$\text{erfc}(x) = \frac{2}{\sqrt{\pi}} \int_{x}^{\infty} \exp(-t)\, dt \qquad \text{(A.6)}$$

is obtained from the relationship erfc(x) = 1 - erf(x). But if the complementary error function is always calculated in this way, there will be large round-off errors as erf(x) approaches unity. Thus, this method has the same useful range of arguments as the error function. However, evaluation of the erfc(x) function for large arguments is frequently required.

One solution to this problem (Reference 22: 329-336) is to calculate the erfc(x) by means of an asymptotic expansion. The resulting equation, expressed as a continued fraction, is

$$\text{erfc}(x) = \frac{1/(1+v/\{1+2v/[1+3v/(1+\cdots)]\})}{\sqrt{\pi}\ x\ \exp\{x^2\}} \qquad \text{(A.7)}$$

where $v = 1/(2x^2)$. For an argument of 1.39, the value for erfc(x) is accurate to 5 significant figures. This algorithm becomes more accurate

as the argument increases.

Pascal Program

The Pascal program given in Figure A.2 calculates erfc(x) for non-negative entries. The calculation of erfc(x) is performed by a set of four functions: POWER (x,n), FINDERF (x), FINDERFC (x), and ERFC (x) where x and n are the required real arguments. Thus, the calculation of erfc(x) may easily be incorporated in any Pascal program by simply including these four modules.

POWER (x,n) is a simple supporting function to aid in the calculation of erfc(x). This function is described below:

POWER (x,n). This function calculates the value of argument x raised to power n.

FINDERF (x), FINDERFC (x), and ERFC (x) are the essential functions for the calculation of erfc(x). These three functions consist of a decision control function, an error function calculator for small arguments, and a complementary error function calculator for larger arguments. These functions are described below:

FINDERF (x). This function calculates values for the error function for arguments less than 1.39. The truncated infinite-series expansion of erfc(x) is used. The complement may be obtained by subtraction from unity with accuracy out to five places.

FINDERFC (x). This function calculates the asymptotic expansion of the complementary error function for large arguments. Results are accurate to five places and become more accurate as the argument is increased.

ERFC (x). This function is the control module. This function is

the one which is called by the main program to compute erfc(x). For arguments in the range 0.035 ≤ x ≤ 1.39, ERFC (x) calls FINDERF (x). The value of the error function is returned and the result for erfc(x) is obtained by subtracting the received value from unity. For arguments greater than or equal to 1.39, ERFC (x) calls FINDERFC (x). Besides providing decision-making, this function also offers error protection. In order to avoid underflow errors, this function sets ERFC(x) equal to unity for arguments less than 0.035 and sets the result equal to zero for arguments greater than 9.23. Negative values should be safeguarded against in the main program; however, should a negative value be encountered, ERFC (x) will display an error message warning the user of an erroneous data point.

```
PROGRAM:  complementary error function
NAME OF PROGRAMMER:  1Lt Steven E. Payne
MAIN MODULE NAME:  complementaryerf

MODULE DESCRIPTION:

        -  This module computes the value of the
        complementary error function for a given
        argument.  The argument must be non-negative.

DESCRIPTION OF ALGORITHM DEVELOPMENT:

        -  Repeat until finished

           -- Read in argument

           -- Calculate erfc(x)

           -- Write answer to screen

           -- Ask user if finished

LOCAL variABLE IDENTIFIER:  x,answer  real
PURPOSE:  Used to calculate complemetary error fcn.
          x = argument    answer = erfc(x)

LOCAL variABLE IDENTIFIER:  finished  BOOLEAN
PURPOSE:  If true then program exits to system.
          If false then program repeats.

LOCAL variABLE IDENTIFIER:  huh
PURPOSE:  Character used to set variable 'finished'.
          User is asked if he would like to quit, if user
          responds with 'y' then 'finished' is set TRUE

LOCAL MODULE CALLED:  erfc(x)
PARAMETERS PASSED:  x
PURPOSE:  Computes the value of the complementary
          error function and prints answer to screen.
```

Fig. A-2. Pascal program for the calculation of the complementary error function, erfc(x).

```
{*************************************************************************}
{*************************************************************************}
{*************************************************************************}



program complementaryerf (  input,output );

var
  x,answer:  real;
  finished:  boolean;
  huh:  char;

{*******************************************************)

function power( base,exponent:  real ): real;
  begin (* power *)
    power := exp ( exponent * ln( base ) )
  end;  (* power *)

{*************************************************************************}

function erf ( x:  real ):  real;
const
  piroot = 1.772453850905;
var
  temp1,temp2,temp3,temp4,temp5 (*,temp6,temp7*) :  real;

begin  (* erf *)
    temp1 := x - power(x,3)/3.0 + power(x,5)/10.0;
    temp2 := -power(x,7)/42.0 + power(x,9)/216.0;
    temp3 := -power(x,11)/1320.0 + power(x,13)/9360.0;
    temp4 := -power(x,15)/75600.0 + power(x,17)/685440.0;
    temp5 := -power(x,19)/6894720.0 + power(x,21)/76204800.0;
{*    temp6 := -power(x,23)/918086400.0 + power(x,25)/11975040000.0;
{*    temp7 := -power(x,27)/168129561600.0;
```

Fig. A-2. Pascal program for the calculation of the complementary error function, erfc(x). (Continued)

```
erf := 2.0/piroot * (temp1 + temp2 + temp3 + temp4 + temp5);
end;  (* erf *)

(*****************************************************************)

function finderfc ( x: real ):  real;
const
  piroot = 1.7724538509;
var
  x2,v,sum:  real;
begin (* finderfc *)
  x2 := x * x;
  v := 1.0/(2.0 * x2);
  sum := v/(1 + 8*v/(1 + 9*v/(1 + 10*v/(1 + 11*v/(1 + 12*v)))));
  sum := v/(1 + 3*v/(1 + 4*v/(1 + 5*v/(1 + 6*v/(1 + 7*sum)))));
  finderfc := 1.0/( exp(x2) * x * piroot * ( 1 + v/(1 + 2*sum)))
end;  (* finderfc *)

(*****************************************************************)

function erfc ( x:  real ):  real;
var
  erfvalue,ec:  real;
begin (* complementary error function *)


    if x < 0.0
      then
        begin
          writeln ('                *** Warning ***');
          writeln ('This program accepts non-negative entries only.');
          writeln ('User attempted to input ',x:10:5);
          writeln ('Recall that erfc(-x) = 2 - erfc(x)');
        end
      else
        begin
          if x < 0.035
          then
            begin
              ec := 1.0;
              erfvalue := 0.0
            end
          else
            begin
              if x < 1.39
                then
                  begin
```

Fig. A-2. Pascal program for the calculation of the complementary error function, erfc(x). (Continued)

```
                    erfvalue := erf(x);
                    ec := 1.0 - erfvalue
                  end
                else
                  begin
                    if x > 9.23
                      then
                        begin
                          ec := 0.0;
                          erfvalue := 1.0
                        end
                      else
                        begin
                          ec := finderfc(x);
                          erfvalue := 1.0 - ec
                        end;
                  end;
              end;
          end;

erfc :=  ec

    end;  (*  error function *)


{*****************************************************************}
{*****************************************************************}
{*******                                                   *******}
{*******              MAIN PROGRAM                         *******}
{*******                                                   *******}
{*****************************************************************}
{*****************************************************************}

begin (* main *)

  finished := false;
  writeln ('This program calculates the complementary error function');

  repeat

  writeln;writeln;
  writeln ('Please enter argument:');
  readln  (x);
  answer := erfc(x);
  if x >= 0.0 then
  begin
    writeln ('  x      = ',x:10:5);
    writeln ('erfc(x) = ',answer:15);
  end;
  writeln;
  writeln('would you like to quit?');
  readln (huh);
  if huh = 'y'
    then finished := true;

  until finished

end.  (* main *)

{*****************************************************************}
```

Fig. A-2. Pascal program for the calculation of the complementary error function, erfc(x). (Continued)

Steven E. Payne was born on 28 July 1959 in Los Angeles, California. He graduated from Branson High School, Branson, Missouri in 1977. In May 1981, he received a Bachelor of Science in Electrical Engineering from the University of Missouri at Rolla and received an Engineer-in-Training Certificate from the State of Missouri. He entered Officer Training School at Lockland AFB, Texas in June 1981 and was commissioned as a Second Lieutenant in the Air Force Reserve in August 1981. He was first assigned to Air Force Institute of Technology's Admissions Directorate as program manager for the Undergraduate Engineering Conversion Program. In June 1982, he entered the Graduate Electrical Engineering Program of AFIT's School of Engineering.

UNCLASSIFIED

SECURITY CLASSIFICATION OF THIS PAGE

REPORT DOCUMENTATION PAGE

1a. REPORT SECURITY CLASSIFICATION UNCLASSIFIED	1b. RESTRICTIVE MARKINGS
2a. SECURITY CLASSIFICATION AUTHORITY	3. DISTRIBUTION/AVAILABILITY OF REPORT Approved for public release; distribution unlimited.
2b. DECLASSIFICATION/DOWNGRADING SCHEDULE	
4. PERFORMING ORGANIZATION REPORT NUMBER(S) AFIT/GE/EE/84J-08	5. MONITORING ORGANIZATION REPORT NUMBER(S)
6a. NAME OF PERFORMING ORGANIZATION School of Engineering	6b. OFFICE SYMBOL (If applicable) AFIT/ENG
6c. ADDRESS (City, State and ZIP Code) Air Force Institute of Technology Wright-Patterson AFB, Ohio 45433	7a. NAME OF MONITORING ORGANIZATION 7b. ADDRESS (City, State and ZIP Code)
8a. NAME OF FUNDING/SPONSORING ORGANIZATION Foreign Technology Div.	8b. OFFICE SYMBOL (If applicable) FTD/TQC
8c. ADDRESS (City, State and ZIP Code) Wright-Patterson AFB, Ohio 45433	9. PROCUREMENT INSTRUMENT IDENTIFICATION NUMBER
11. TITLE (Include Security Classification) Millimeter Wave Communications (U)	10. SOURCE OF FUNDING NOS. PROGRAM ELEMENT NO. / PROJECT NO. / TASK NO. / WORK UNIT NO.

12. PERSONAL AUTHOR(S)
Steven E. Payne, 1st Lt, USAF

13a. TYPE OF REPORT	13b. TIME COVERED	14. DATE OF REPORT (Yr., Mo., Day)	15. PAGE COUNT
MS Thesis	FROM _____ TO _____	1984 June	80

16. SUPPLEMENTARY NOTATION

COSATI CODES			18. SUBJECT TERMS (Continue on reverse if necessary and identify by block number)
FIELD	GROUP	SUB. GR.	Millimeter Waves Communication and Radio Systems Radio Links
17	02	1	

19. ABSTRACT (Continue on reverse if necessary and identify by block number)

ThesisAdvisor: Kenneth G. Castor, Major, USAF

Approved for public release: IAW AFR 190-17.
8 Aug 84
DEAN F. WOLAVER
Dean for Research and Professional Development
Air Force Institute of Technology (AFIT)
Wright-Patterson AFB OH 45433

20. DISTRIBUTION/AVAILABILITY OF ABSTRACT UNCLASSIFIED/UNLIMITED ☒ SAME AS RPT. ☐ DTIC USERS ☐	21. ABSTRACT SECURITY CLASSIFICATION UNCLASSIFIED
22a. NAME OF RESPONSIBLE INDIVIDUAL Kenneth G. Castor, Major, USAF	22b. TELEPHONE NUMBER (Include Area Code) (513) 255-3576
	22c. OFFICE SYMBOL AFIT/ENG

DD FORM 1473, 83 APR EDITION OF 1 JAN 73 IS OBSOLETE.

UNCLASSIFIED
SECURITY CLASSIFICATION OF THIS PAGE

This investigation establishes the maximum communication link, i.e., transmitter/receiver separation, available to a millimeter wave channel in a clear, non-trubulent atmosphere for a low-power, low data-rate system. The frequencies considered are from the oxygen resonant absorbtion band centered around 60 GHz for several altitudes to 20 kilometers. The effort is concerned with various modulation schemes for the transmission of digital data and their relative performance in the presence of a jammer.

The analysis is accomplished by taking the Friis communication link equation and accounting for tropospheric absorbtion loss. A Pascal-coded algorithm is developed to assess the relative data transmission performance of the various modulation techniques. The program was written general enough for the user to specify: the carrier frequency, attenuation factor, transmitter power, transmitting and receiving antenna gains, system bandwidth, particular modulation technique, set of range values of interest, jammer power, jammer's antenna gain, and jammer's location.

The results of this investigation indicate that communication links operating at frequencies centered around 60 GHz of the millimeter wave region end rather abruptly due to the inherently high attenuation. Jamming has a limited effect on millimeter wave communications depending upon the frequency. For the frequencies considered, a jammer requires enormous amounts of power and must be positioned "uncomfortably" close to the target receiver to be effective. The application of coherent modulation methods, coding, or spread spectrum techniques as a means to improve the performance of millimeter waves is not required.